Testing the astronomical time scale for oceanic anoxic event 2, and its extension into Cenomanian strata of the Western Interior Basin (USA)

Chao Ma[1], Stephen R. Meyers[1,†], Brad B. Sageman[2], Brad S. Singer[1], and Brian R. Jicha[1]
[1]*Department of Geoscience, University of Wisconsin–Madison, 1215 West Dayton Street, Madison, Wisconsin 53706, USA*
[2]*Department of Earth and Planetary Sciences, Northwestern University, 2145 Sheridan Road, Evanston, Illinois 60208, USA*

ABSTRACT

The development of integrated astronomical and radioisotopic time scales from rhythmic strata of the Western Interior Basin (WIB) has played a fundamental role in the refinement of Late Cretaceous chronostratigraphy. In this study, X-ray fluorescence (XRF) core scanning is utilized to develop a new elemental data set for cyclostratigraphic investigation of Cenomanian-Turonian strata in the WIB, using material from the Aristocrat-Angus-12-8 core (north-central Colorado). The XRF data set yields the first continuous 5-mm-resolution analysis of lithogenic, biogenic, and syngenetic-authigenic proxies through the uppermost Lincoln Limestone Member, the Hartland Shale Member, and the Bridge Creek Limestone Member, including oceanic anoxic event 2 (OAE 2). The $^{40}Ar/^{39}Ar$ ages from ashes in three biozones, including a new age from the *Dunveganoceras pondi* biozone (uppermost Lincoln Limestone Member), provide geochronologic constraints for the cyclostratigraphic analysis. Astrochronologic testing of the 5-mm-resolution XRF weight percent $CaCO_3$ data via average spectral misfit analysis yields strong evidence for astronomical influence on climate and sedimentation. Results from the Bridge Creek Limestone Member are consistent with the previously published astrochronology from the U.S. Geological Survey #1 Portland core (central Colorado), and identification of an astronomical signal in the underlying Hartland Shale Member now permits extension of the WIB astrochronology into the earlier Cenomanian, prior to OAE 2. High rates of sedimentation in the Angus core during the interval of OAE 2 initiation, as compared to the Portland core, allow recognition of a strong precessional control on bedding development. As a consequence, the new results provide a rare high-resolution chronometer for the onset of OAE 2, and the timing of proposed hydrothermal trace metal enrichment as observed in the 5 mm XRF data.

INTRODUCTION

The Cenomanian-Turonian boundary interval (ca. 94 Ma; Meyers et al., 2012a) records oceanic anoxic event 2 (OAE 2), a major biogeochemical perturbation to the Earth system. The event is characterized by widespread deposition of organic-carbon–rich strata and a positive carbon isotope excursion (Pratt, 1985; Arthur et al., 1985, 1988; Schlanger et al., 1987; Hayes et al., 1989; Arthur and Sageman, 1994; Sageman et al., 1997, 2006; Paul et al., 1999; Wang et al., 2001; Tsikos et al., 2004; Bowman and Bralower, 2005; Jarvis et al., 2006; Li et al., 2006; Elrick et al., 2009), and it is associated with the extinction of a variety of molluscs, planktic foraminifera, and nannoplankton (Elder, 1989; Premoli-Silva et al., 1999; Leckie et al., 2002; Erba, 2004). A detailed understanding of the mechanisms underlying OAE 2, and accurate calculation of biogeochemical and paleobiologic rates across the event require high-resolution time scales, even exceeding what is possible using radioisotopic geochronology and biostratigraphy (Sageman et al., 2006; Meyers et al., 2012a). Astrochronology is a potential tool for construction of the necessary high-resolution geological time scales (Hinnov, 2000), and consequently cyclostratigraphic analyses of various OAE 2 deposits have been conducted (e.g., Kuhnt et al., 1997, 2004; Gale et al., 1999; Caron et al., 1999; Prokoph et al., 2001; Kuypers et al., 2004; Sageman et al., 2006; Voigt et al., 2008; Meyers et al., 2001, 2012a, 2012b).

Within the Western Interior Basin, cyclostratigraphic work on the Cenomanian-Turonian boundary initiated with Gilbert (1895). Gilbert was the first to hypothesize a correlation between climate changes driven by Earth's orbit and lithologic cycles, such as those preserved in the rhythmically bedded strata of the Bridge Creek Limestone Member, Greenhorn Formation, in central Colorado. Fischer (1980) revived interest in the Colorado bedding cycles, and Sageman et al. (1997, 1998) provided the first spectral analyses of geochemical, lithologic, and paleobiologic data that yielded quantitative evidence for the existence of astronomical forcing in Cenomanian-Turonian sequences of the Western Interior Basin. This work primarily focused on strata immediately following OAE 2, in the upper Bridge Creek Limestone Member, because changing sedimentation rates in the OAE 2 interval led to complex bedding patterns that were more difficult to analyze. To address this issue, Meyers et al. (2001) subsequently applied a "time-frequency" cyclostratigraphic methodology termed evolutive harmonic analysis (EHA) to high-resolution grayscale data from the Bridge Creek Limestone Member, allowing quantification of an astronomical influence in the OAE 2 interval and development of a detailed astronomically derived sedimentation rate history for the entire Bridge Creek Limestone Member in the U.S. Geological Survey (USGS) #1 Portland core. Combining the new astrochronology with existing radioisotopic data, updated biostratigraphy, and a new high-resolution carbon isotope record, Sageman et al. (2006) established a comprehensive chronostratigraphy for the Cenomanian-Turonian global stratotype section and point (GSSP) in the Pueblo, Colorado, region. These results better constrain the timing and duration of the OAE 2 carbon isotope excursion and the constituent biozones, which form the basis of global chronostratigraphy for this interval. Subsequently, the OAE 2 time scale of Sageman et al. (2006) was revised via intercalibration with new $^{40}Ar/^{39}Ar$ and U-Pb radioisotopic data from the Western Interior Basin by Meyers et al. (2012a).

The major remaining uncertainty in OAE 2 cyclostratigraphy from the Western Interior Basin is associated with the transition into the positive carbon isotope excursion, which commences in the upper part of the Hartland Shale

†E-mail: smeyers@geology.wisc.edu.

GSA Bulletin; July/August 2014; v. 126; no. 7/8; p. 974–989; doi: 10.1130/B30922.1; 8 figures; 4 tables; Data Repository item 2014136; published online 20 March 2014.

Member. Since the existing Western Interior Basin cyclostratigraphy begins immediately above the basal limestone bed of the overlying Bridge Creek Limestone Member (referred to as "LS1" by Elder, 1985), just following the initiation of the carbon isotope excursion, assumptions about the duration of LS1 and extrapolation into the uppermost ~30 cm of Hartland Shale in the USGS #1 Portland core are necessary to determine OAE 2 duration. Furthermore, at both the Pueblo type section and in the USGS #1 Portland core, the interval immediately below LS1 includes a conspicuous skeletal bed that may represent a hiatus. The skeletal bed precedes an interval interpreted to represent a major transgression in the basin, based on a 170 km retreat of shoreface deposits on the western margin of the basin that correlates with the deposition of LS1 (Kauffman, 1977; Hook and Cobban, 1981; Elder, 1985; Hattin, 1986; Sageman, 1996; Meyers et al., 2001). Our ability to definitively assess the tempo of the initial onset of the OAE 2 carbon isotope excursion within the Western Interior Basin is thus limited by poor constraint on the magnitude of the potential hiatus, on the rate of sedimentation within the uppermost Hartland Shale Member, and on the temporal duration of LS1.

To address these issues, we initiated a cyclostratigraphic study of the Aristocrat-Angus-12-8 core from northern Colorado (Locklair and Sageman, 2008). This core is of particular interest because the OAE 2 interval appears to preserve a more-continuous and complete transition from the Hartland Shale Member into the lower Bridge Creek Limestone Member during OAE 2 initiation. This provides an opportunity to (1) better quantify the cyclostratigraphy and biogeochemistry of the transition into the OAE 2, (2) test the veracity of the published Cenomanian-Turonian boundary astrochronology (Meyers et al., 2001, 2012a; Sageman et al., 2006) at another location within the Western Interior Basin, (3) explore the feasibility of extending the astrochronology into the earlier Cenomanian Hartland Shale Member and Lincoln Limestone Member, and (4) integrate the astronomical time scale (ATS) with published and emerging radioisotopic and chemostratigraphic data from the Western Interior Basin to better constrain Late Cretaceous geochronology and chronostratigraphy.

The primary data for our astrochronologic assessment were generated using X-ray fluorescence (XRF) core scanning, which allows geochemical variability to be quantified at 5 mm resolution for the entire Bridge Creek Limestone Member, the Hartland Shale Member, and uppermost Lincoln Limestone Member. This XRF data set provides the first continuous 5-mm-resolution analysis of lithogenic, biogenic, and syngenetic-authigenic proxies through the interval of Western Interior Basin strata examined here, including OAE 2. Integration of the XRF data with weight percent $CaCO_3$ data and carbon isotopic measurements ($\delta^{13}C_{org}$) from the same core (Joo et al., 2014) provides a comprehensive data set for correlation and comparison of our results with the well-studied USGS #1 Portland core (Sageman et al., 1997, 1998, 2006; Sageman and Lyons, 2003; Meyers et al., 2012a).

To test for astronomical influence in the Angus core XRF data, we utilized two approaches: the recently developed evolutive average spectral misfit method (evolutive ASM; Meyers et al., 2012b), and an adaptation of the ASM technique that is suitable for the evaluation of data series characterized by a relatively weak but pervasive stratigraphic expression of astronomical signals (a low signal:noise ratio). The latter approach is designed to enhance statistical power (the ability to detect astronomical influence when it is indeed present) while also decreasing the number of "false positive" spectral peaks (e.g., Meyers, 2012). This adaptation of the ASM method is a key step in extending the existing Western Interior Basin astronomical time scale (Meyers et al., 2001; Sageman et al., 2006) into the late Cenomanian Hartland Shale Member, where the lithologic rhythms are not as clearly or consistently expressed as in the overlying Bridge Creek Limestone Member. The combination of the two ASM approaches is critical for the calibration of astronomical signals in the Angus core, as well as the identification of stratigraphic intervals where astronomical influence cannot be confirmed and caution should be exercised.

As will be demonstrated herein, results from the new Angus core ATS are consistent with the previously published OAE 2 astrochronology from the USGS #1 Portland core (Meyers et al., 2001; Sageman et al., 2006). In general, the Portland core ATS demonstrates a higher astronomical signal:noise ratio for the Bridge Creek Limestone Member (Meyers et al., 2001), and thus a better constrained astrochronology. However, the Angus core reveals a higher-resolution precession-scale chronometer during the onset of OAE 2, due to expanded deposition at this particular location, and it also allows extension of the ATS ~1 m.y. prior to OAE 2. An additional highlight from our analysis of the Angus core is a continuous XRF elemental data set for evaluation of the timing of proposed hydrothermal trace metal enrichment associated with OAE 2 (Orth et al., 1993; Leckie et al., 2002; Snow et al., 2005; Turgeon and Creaser, 2008). The new XRF data set supports a two-phase magmatic pulse model for OAE 2, as proposed by Turgeon and Creaser (2008), and provides better constraints on the timing of the magmatic events.

MATERIAL AND METHODS

Material: Aristocrat-Angus-12-8 Core and *Dunveganoceras pondi* Ash Bed

Located in the Wattenerg field on the west side of the Denver Basin (north-central Colorado; Fig. 1), the Aristocrat-Angus-12-8 ("Angus") core was drilled in 2003 by EnCana Oil and Gas (U.S.A.). Within the core, the Bridge Creek Limestone Member consists of interbeds of calcareous shale or marlstone with either marlstone or limestone (Fig. 2). The Hartland Shale Member is primarily composed of calcareous shale with occasional calcarenite layers, but a greater abundance of calcarenites occurs in the middle portion of the unit (Fig. 2). The thickness of the Bridge Creek Limestone Member in the Angus core is 15.99 m, and the Hartland Shale Member is 18.68 m (both including bentonite layers). This compares to 11.80 m of Bridge Creek Limestone Member and 12.80 m of Hartland Shale Member in the USGS #1 Portland core (Dean and Arthur, 1998; Meyers et al., 2001; Sageman et al., 2006), indicating expanded deposition in the Angus core. In addition to the Bridge Creek Limestone Member and Hartland Shale Member, our cyclostratigraphic analysis includes the uppermost Lincoln Limestone Member, which is composed of interbedded calcarenitic limestone, marlstone, and calcareous shale (Fig. 2).

Sanidine extracted from bentonite in the *Dunveganoceras pondi* ammonite zone of the Frontier Formation in Carter County, Wyoming (sample D2315 of Obradovich, 1993), was reanalyzed for the present study. In central Colorado, the *D. pondi* biozone occurs in the uppermost Lincoln Limestone Member, and it is placed in the lowermost portion of the analyzed Angus core stratigraphy (Fig. 2). Since dated bentonite horizons from the lower Bridge Creek Limestone Member in the Pueblo GSSP (Meyers et al., 2012a) can be correlated to the Angus core (Fig. 3), there is radioisotope age constraint at both the base and top of the study interval.

Methodology: X-Ray Fluorescence Core Scanning

The elements aluminum, silicon, calcium, manganese, iron, and copper were measured at 5 mm × 5 mm resolution using the University of Wisconsin–Madison Avaatech X-ray fluorescence core scanner (Richter et al., 2006). Elements were measured with a 10 kV accelera-

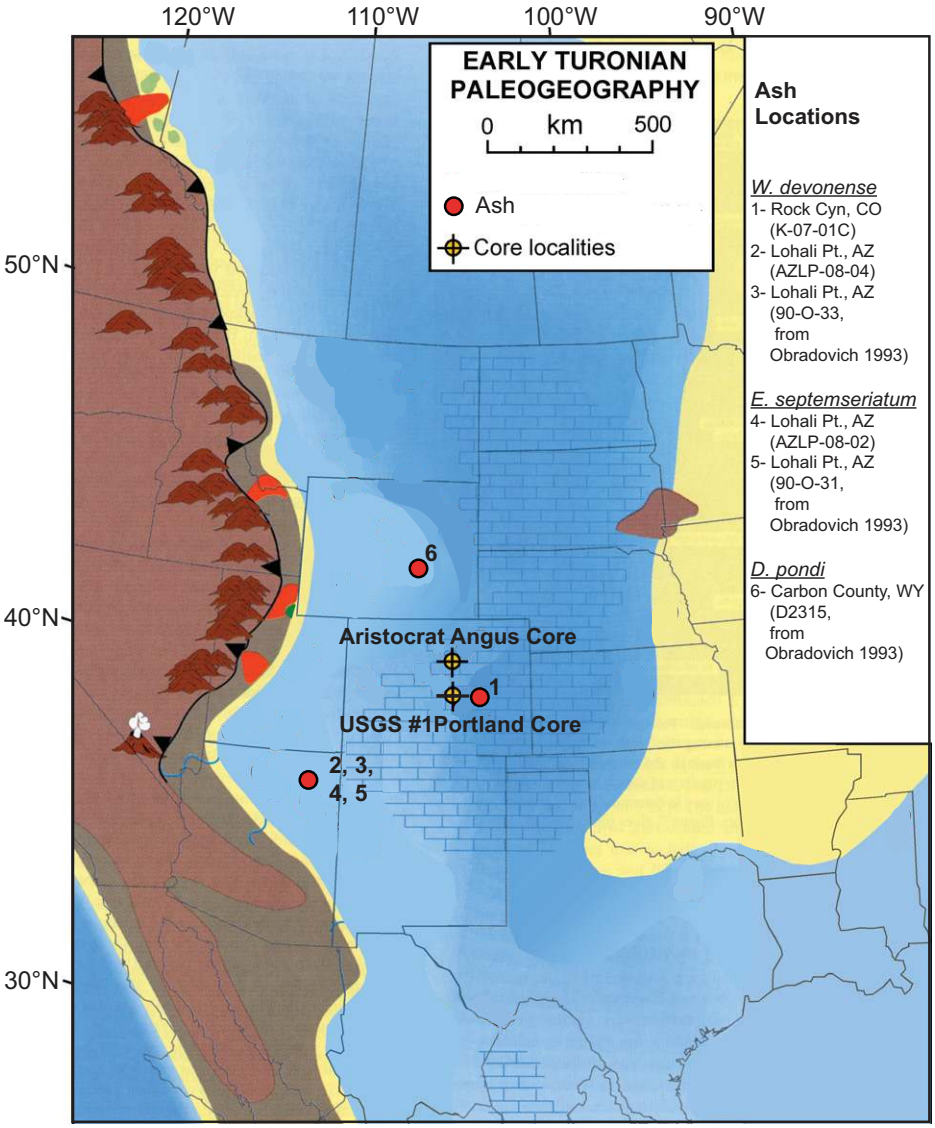

Figure 1. Paleogeographic map of the Western Interior Basin for the mid-Cretaceous (94 Ma) (modified from Roberts and Kirschbaum, 1995), illustrating the location of the Aristocrat Angus 12-8 core and the USGS #1 Portland core, previously studied by Sageman et al. (1997), Meyers et al. (2001), and Sageman et al. (2006). Also identified are the locations of the ash beds that are utilized for radioisotopic geochronology. Sample codes follow the designations provided in Obradovich (1993) and Meyers et al. (2012a). *W. devonense—Watinoceras devonense*, *E. septemseriatum—Euomphaloceras septemseriatum*, *D. pondi—Dunveganoceras pondi*.

tion voltage (1000 µA source current, no filter, 10 s measurement time), with the exception of copper, which was measured using a 30 kV acceleration voltage (2000 µA source current, thick-palladium filter, 10 s measurement time). Data reduction and spectrum evaluation were conducted with the software WinAxil v. 4.5.2. To assess the stability of the XRF scanning analyses over the period of the study, 260 standard measurements ("SARM 4"; Potts et al., 1992) were performed before and after most scans, and these demonstrated exceptional stability (e.g., the coefficient of variation for Ca is 0.01; GSA Data Repository supplementary Fig. 1[1]). Additionally, >1100 duplicate analyses of Angus core material indicate an analytical uncertainty of <2% for most of the investigated elements and provide important information relevant to our subsequent interpretation of the data set (supplementary Table 1 and supplementary Fig. 2 [see footnote 1]).

For this study, calcium XRF count data were quantitatively calibrated to weight percent calcium carbonate content using 66 CO_2 coulometry measurements (Joo et al., 2014; for methodology, see Huffman, 1977). The 10–15-mm-thick core segments analyzed by CO_2 coulometry typically span multiple 5 mm Ca XRF measurements (supplementary Fig. 3 [see footnote 1]), the latter of which were averaged for comparison. The resulting linear calibration equation (Pearson correlation coefficient, $r = 0.97$) was utilized to convert all XRF Ca count data to wt% $CaCO_3$ (Fig. 2A). As documented in the following, the astrochronologic analysis is primarily concerned with these calibrated wt% $CaCO_3$ data, which are inversely correlated with lithogenic aluminum ($r = –0.93$) and silicon ($r = –0.92$) contributions (Figs. 2B and 2C; see Angus Core XRF Scanning Results section). Manganese and iron XRF count data were utilized to aid in chemostratigraphic correlation of the Angus core with the USGS #1 Portland core; relevant to this issue, both manganese and iron document important time-correlative authigenic-syngenetic geochemical shifts, which have been previously established within the basin (Sageman and Lyons, 2003; Meyers et al., 2005; Meyers, 2007). The manganese and iron data were supplemented by copper XRF data to further evaluate the hydrothermal trace metal enrichment that has been proposed for OAE 2 deposits (Orth et al., 1993; Snow et al., 2005).

Methodology: $^{40}Ar/^{39}Ar$ Geochronology

Thirty-three $^{40}Ar/^{39}Ar$ single-crystal laser fusion ages were determined from the *D. pondi* ash (sample D2315 of Obradovich, 1993), at the University of Wisconsin–Madison. The analytical methodology followed that of Meyers et al. (2012a), with minor modification as outlined in Sageman et al. (2014). The age is reported with analytical uncertainties at the 95% confidence level, and total uncertainties (analytical, ^{40}K decay constant, and Fish Canyon sanidine standard age) at 2σ (Tables 1 and 2; supplementary Table 3 [see footnote 1]), and they were calculated relative to a Fish Canyon standard age of 28.201 ± 0.046 Ma (Kuiper et al., 2008) and a value for $\lambda^{40}K$ of $5.463 \pm 0.107 \times 10^{-10}$ yr^{-1} (Min et al., 2000). See Schmitz (2012) for justification of these values.

Methodology: Astrochronologic Testing

The calcium XRF data provide several specific advantages for our astrochronologic assessment. First, previous studies have demon-

[1]GSA Data Repository item 2014136, Geochemical data and astrochronologic testing results, is available at http://www.geosociety.org/pubs/ft2014.htm or by request to editing@geosociety.org.

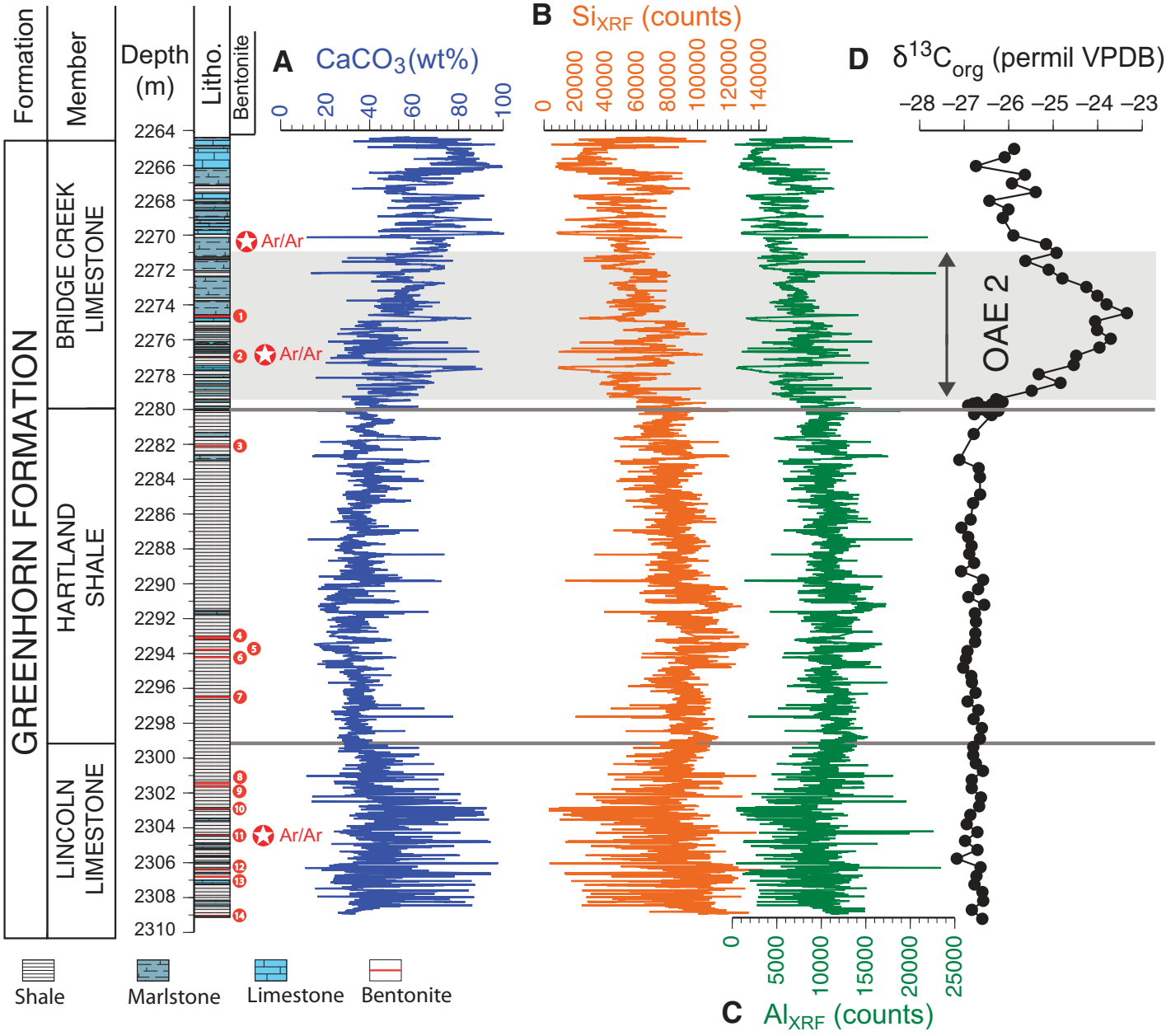

Figure 2. Detailed stratigraphy for the Angus core, plotted with 5-mm-resolution wt% $CaCO_3$, Si_{XRF}, Al_{XRF}, and $\delta^{13}C_{org}$ data. The numbered circles to the right of the stratigraphic column identify bentonite layers, and the three stars indicate the stratigraphic location of dated ash beds that have been correlated into the Angus core for geochronologic constraints. (A) Calibrated XRF wt% $CaCO_3$ profile from this study, (B) X-ray fluorescence (XRF) scanning results for Si (counts). (C) XRF scanning results for Al (counts). (D) Bulk organic carbon isotope data from Joo et al. (2014). The shaded area indicates the interval of oceanic anoxic event (OAE) 2. VPDB—Vienna Peedee belemnite.

strated that wt% $CaCO_3$ preserves a strong astronomical signal in the Bridge Creek Limestone Member (Sageman et al., 1997, 1998; Meyers and Sageman, 2007; Meyers et al., 2001), and possibly also in the underlying Hartland Shale Member (Gale et al., 2008). Second, there are numerous plausible mechanisms that have been proposed to link carbonate concentration and astronomical forcing in Cretaceous deposits, including astronomically influenced changes in carbonate production, in siliciclastic dilution, or in some combination of both (Arthur et al., 1984; Eicher and Diner, 1985, 1989, 1991; Arthur and Dean, 1991; Pratt et al., 1993; Sageman et al., 1997). A third advantage is excellent analytical reproducibility of the Ca XRF analyses (supplementary Table 1 [see footnote 1]), and the availability of wt% $CaCO_3$ measurements for calibration of the Ca XRF count data directly to quantitative wt% $CaCO_3$ data (Joo et al., 2104). Finally, carbonate and clay/silt fractions represent the two major codiluting sedimentary components in these hemipelagic strata (followed by organic matter and sulfides; Dean and Arthur,

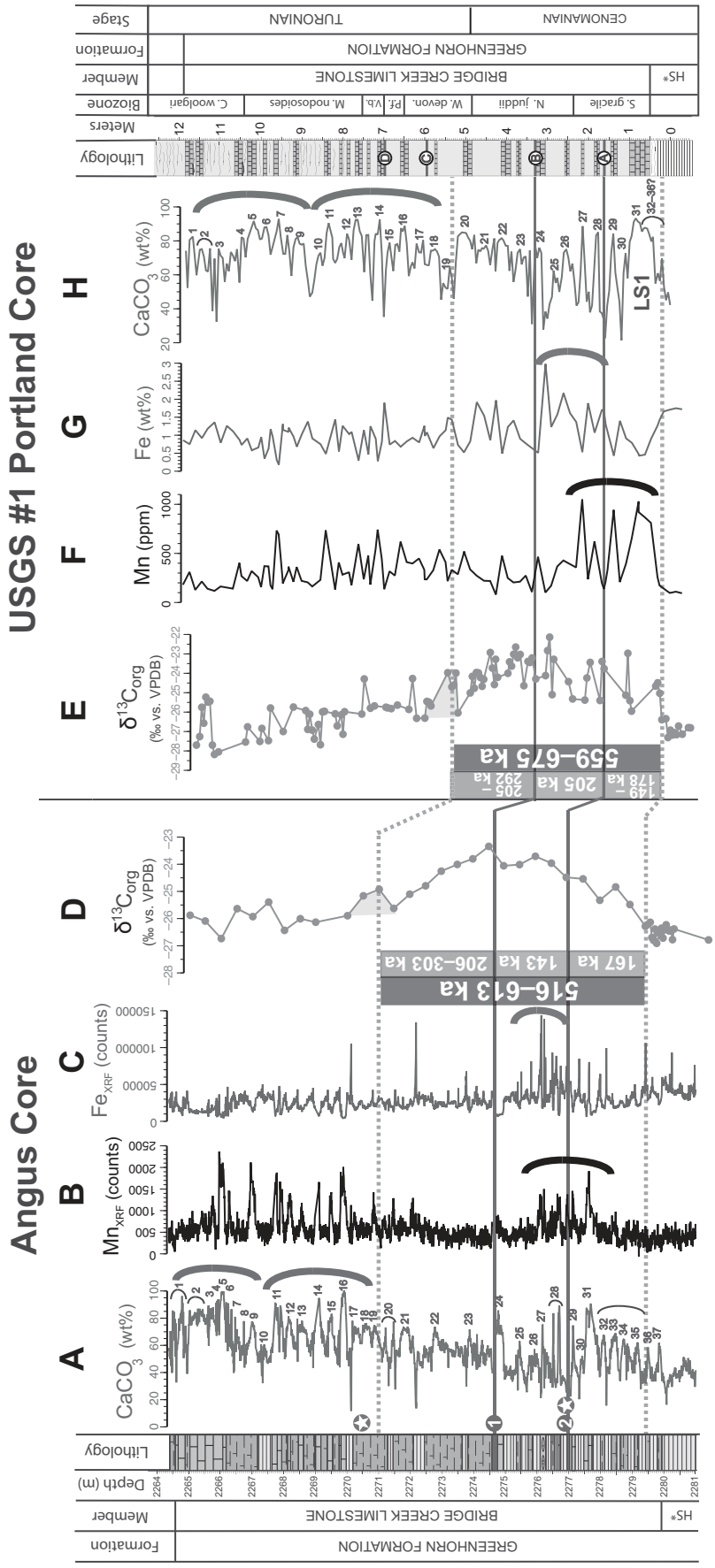

Figure 3. Correlation of the Angus core to the USGS #1 Portland core, using lithostratigraphy, $CaCO_3$, Mn, Fe, and $\delta^{13}C_{org}$ data. For the Angus core, plotted to the right of Bridge Creek Limestone Member lithostratigraphy are: (A) calibrated wt% $CaCO_3$ content, (B) X-ray fluorescence (XRF) scanning results for Mn (counts), (C) XRF scanning results for Fe (counts), and (D) bulk organic carbon isotopes (‰ vs. Vienna Peedee belemnite [VPDB]; Joo et al., 2014). For the USGS #1 Portland core, plotted to the left of Bridge Creek Limestone Member lithostratigraphy (after Meyers et al., 2012a) are: (E) bulk organic carbon isotopes (‰ vs. VPDB; Sageman et al., 2006), (F) Mn content (ppm; Sageman and Lyons, 2003), (G) Fe content (wt%; Sageman and Lyons, 2003), and (H) wt% $CaCO_3$ (Sageman et al., 1997). Adjacent to the Angus core lithostratigraphy, the circles with numbers 1 and 2 are bentonite layers correlated to bentonite layers "B" and "A" (respectively) in the Portland core. The two dotted lines identify the initiation and termination of the oceanic anoxic event (OAE) 2 based on available $\delta^{13}C_{org}$ data (the shaded area for the upper correlation indicates uncertainty in our placement of the termination). Numbers adjacent to the wt% $CaCO_3$ records from the Angus core and Portland core demarcate the proposed high-resolution correlation. Legend for the Angus core lithology is the same as in Figure 2. Legend for the Portland core lithology follows Sageman et al. (2006). HS—Hartland Shale. *S. gracile—Sciponoceras gracile, N. juddii—Neocardioceras juddii, W. devon.—Watinoceras devonense, Pf.—Pseudaspidoceras flexuosum, V.b.—Vascoceras birchbyi, M. nodosoides—Mammites nodosoides, C. woolgari—Collignoniceras woollgari.*

TABLE 1. SEDIMENTATION RATE CONSTRAINTS FOR THE ANGUS CORE ASTROCHRONOLOGIC TESTING, BASED ON RADIOISOTOPICALLY DATED BENTONITES

Biozone	Age* (Ma)	Position in Angus core† (m)	Duration (m.y.)	Thickness (m)	Sedimentation rate (cm/k.y.)
Watinoceras devonense	93.79 ± 0.12 (Meyers et al., 2012a)	2269.95–2270.95	0.41 ± 0.19	6.30 ± 0.50	0.96–3.12
Euomphaloceras septemseriatum	94.20 ± 0.15 (Meyers et al., 2012a)	2276.75			
Dunveganoceras pondi	95.39 ± 0.18	2300.76–2308.13	1.19 ± 0.23	27.70 ± 3.68	1.69–3.28

*Analytical uncertainty at the 95% confidence level.
†Position corrected for removal of bentonite thicknesses.

1989; Sageman et al., 1997); therefore, wt% $CaCO_3$ provides a reliable measure of major changes in the lithologic character of the strata.

Accurate characterization of astronomical influence on climate and deposition using the Angus core XRF data is potentially complicated by interference with stochastic climate processes, unsteady sedimentation, and a range of other competing factors (Meyers et al., 2001, 2008; Weedon, 2003). Thus, the evaluation of astronomical signals requires application of a series of quantitative methodologies that are capable of constraining sources of noise, as well as the use of appropriate statistical criteria to explicitly test astronomical hypotheses. In this study, we used a multifaceted approach for astrochronologic assessment to optimize astronomical signal detection in the presence of multiple noise sources. First, prior to time-series analysis of the calibrated wt% $CaCO_3$ XRF data set, 14 bentonite layers were removed (Fig. 2). Their identification was based on visual evaluation of the core and examination of the 5 mm XRF geochemical data. Since volcanic ash layers are deposited relatively instantaneously, they are not expected to record changes in "background" sedimentation that are sensitive to astronomically forced climate variations.

Evolutive harmonic analysis (EHA) and evolutive power spectral analysis (EPSA) (Meyers et al., 2001; Meyers and Hinnov, 2010) were applied to evaluate changes in the character of spatial bedding cycles throughout the Angus core wt% $CaCO_3$ XRF record. EHA and EPSA were implemented using a 7 m moving window (0.1 m step), experimentally determined to be an optimal size to assess the temporal evolution of spectral features in the wt% $CaCO_3$ XRF data. To constrain the possible temporal duration of the observed spatial cycles, a range of plausible sedimentation rates for the strata was determined using a new $^{40}Ar/^{39}Ar$ radioisotopic age from the *Dunveganoceras pondi* biozone in the uppermost Lincoln Limestone Member, in addition to recently published radioisotopic data from the Bridge Creek Limestone Member (Meyers et al., 2012a).

Using the 7 m window EHA/EPSA results and the radioisotopic-based sedimentation rate constraints as a guide, ASM analysis was then applied to provide a quantitative test of astronomical influence at different stratigraphic levels (Meyers and Sageman, 2007; Meyers et al., 2012b). The ASM approach has some philosophical similarities with the commonly employed "ratio method" (e.g., the ~5:2:1 relationship among ~100 k.y. short eccentricity, the ~40 k.y. obliquity component, and the ~20 k.y. precession component). However, in contrast to the ratio method, ASM explicitly formulates astronomical testing as an inverse problem, where time scale uncertainty is evaluated, and Monte Carlo simulation provides a means by which to test the null hypotheses of no astronomical influence (for a Bayesian approach, see Malinverno et al., 2010). The ASM Monte Carlo significance levels can alternatively be considered as indicating the probability that the observed bedding cycles are derived by chance arrangement of "false positive" peaks in the spectrum (Meyers, 2012).

We used two ASM-based approaches to evaluate the Angus core data: evolutive ASM (Meyers et al., 2012b), and an adaptation of the ASM method that is designed for detection of weak but pervasive astronomical signals. Importantly, the evolutive ASM method provides a means by which to prospect for portions of the stratigraphic record characterized by a high astronomical signal:noise ratio. The method is implemented as a "sliding window" ASM analysis, using all harmonic components ≥90% F-test confidence level (Thomson, 1982) from each 7 m EHA window.

An adaptation of the ASM method was subsequently used to evaluate portions of the wt% $CaCO_3$ record that were characterized by a comparatively low signal:noise ratio. The first step in this approach is to use the 7 m EHA and EPSA results to identify broader segments of the stratigraphic record that express stable bedding cycles. This yields a longer stratigraphic "window" with a greater potential for identification of the full suite of astronomical signals, especially the low-frequency eccentricity terms. Three criteria are then used to select candidate bedding cycles for astrochronologic testing from this longer interval: (1) The specific bedding cycle must be relatively stable and persistent in the EHA and EPSA results, (2) the harmonic F-test confidence level must be ≥80% in the total MTM (multitaper method) spectrum for the stratigraphic interval and also in the EHA results, and (3) the bedding cycle must have high amplitude and power relative to the local background in the MTM spectrum. This approach allows for the fact that individual astronomical terms (eccentricity, obliquity, precession) wax and wane in their strength due to amplitude modulation (Laskar et al., 2004, 2011); thus, in stratigraphic data with a relatively weak expression of the astronomical cycles, the expected eccentricity, obliquity, and precession signals may not simultaneously achieve high significance in a given 7 m EHA window, which is required for successful identification using the evolutive ASM approach.

It should be noted that reduction of the required harmonic F-test confidence level threshold from 90% to 80% in this analysis lowers the degree of phase coherence (lower signal:noise) required for signal identification, but it does not necessarily increase the likelihood of identifying an astronomical signal using ASM. More specifically, lowering the harmonic F-test confidence level threshold increases the number of spectral frequencies evaluated

TABLE 2. SUMMARY OF $^{40}Ar/^{39}Ar$ SINGLE-CRYSTAL SANIDINE FUSIONS

Biozone	Sample	N	MSWD	Weighted mean age* Age (Ma)	95%†	±2σ§
Dunveganoceras pondi	D2315	25 of 33	0.69	95.39	±0.18	±0.37

*Age calculated relative to 28.201 Ma for Fish Canyon sanidine (Kuiper et al., 2008) using Min et al. (2000) decay constant.
†Analytical uncertainty at the 95% confidence level.
§Fully propagated uncertainty (includes decay constant, analytical uncertainties, and Fish Canyon sanidine standard age).

by ASM, potentially allowing for a better fit to the astronomical model, but it also increases the number of frequencies utilized in the Monte Carlo spectra simulations, making it more difficult to reject the null hypothesis of "no astronomical signal" (especially if the additional spectral peaks are false positives). Thus, the ASM method has a built-in safeguard against false astronomical signal identification, regardless of the specific harmonic F-test confidence level threshold that is applied.

The theoretical target periods (eccentricity-tilt-precession; henceforth ETP model) for all ASM analyses were derived from the astronomical model of Laskar et al. (2004, 2011), and their uncertainty assessment has been previously presented in Meyers et al. (2012b) (supplementary Table 2 [see footnote 1]). ASM hypothesis testing was conducted with 100,000 Monte Carlo simulated spectra, utilizing the same number of "significant" frequencies identified in each measured wt% $CaCO_3$ spectrum (see Meyers et al., 2012b). Two-hundred individual sedimentation rates were evaluated, on a logarithmic grid, yielding a critical null hypothesis (H_o) significance level of 0.5%.

ANGUS CORE XRF SCANNING RESULTS

Figure 2 presents the XRF calibrated wt% $CaCO_3$ data and aluminum and silicon count data for the entire study interval, along with lithostratigraphy and $\delta^{13}C_{org}$ measurements from the core (Joo et al., 2014). Important features of this data set include: (1) reciprocal oscillatory sedimentologic variability between biogenic (wt% $CaCO_3$) and lithogenic (aluminum and silicon) components throughout the entire study interval, including the more carbonate-poor Hartland Shale Member, (2) especially pronounced oscillations of wt% $CaCO_3$ in the carbonate-rich Bridge Creek Limestone Member and Lincoln Limestone Member, and (3) an ~4‰ positive $\delta^{13}C_{org}$ excursion that defines OAE 2, with little variability during deposition of the Hartland Shale and Lincoln Limestone Members.

Manganese content shows the greatest enrichment in two stratigraphic intervals of the core, both of which occur in the Bridge Creek Limestone (Fig. 3B; full data set is presented in supplementary Fig. 4 [see footnote 1]). The first stratigraphic interval of enhanced Mn content is manifested as regularly occurring Mn enrichments within carbonate-rich beds of the upper Bridge Creek Limestone (Fig. 3B). The second interval is a more localized Mn enrichment (henceforth, "OAE 2 enrichment") within the lower half of the $\delta^{13}C_{org}$ excursion that defines OAE 2 (Fig. 3D), and Mn content in this interval exhibits no clear preference for limestone or shale beds.

Iron content demonstrates a substantial linear correlation with lithogenic components aluminum (r = 0.85) and silicon (r = 0.76) (supplementary Fig. 4 [see footnote 1]), but it also displays some degree of decoupling from the lithogenic fraction. In this regard, the most obvious feature in the Bridge Creek Limestone is an enhanced iron content within the lower half of the $\delta^{13}C_{org}$ excursion that is decoupled from lithogenic inputs (Fig. 3C). This iron enrichment and the aforementioned manganese OAE 2 enrichment have been previously identified in the USGS #1 Portland core (Sageman and Lyons, 2003; Meyers et al., 2005; Meyers, 2007) and will be utilized as chronostratigraphic markers in the following section (Stratigraphic Correlation of Angus Core to the USGS #1 Portland Core). The copper XRF data, while displaying more scatter than the other elements (largely due to lower count rates, decreasing the signal:noise ratio; supplementary Table 1 and supplementary Fig. 2 [see footnote 1]), demonstrate a marked increase within the same interval that displays iron enrichment (supplementary Fig. 4 [see footnote 1]). An enrichment in copper within this same stratigraphic interval has been previously identified in lower-resolution data from the Rock Canyon anticline section (Snow et al., 2005).

STRATIGRAPHIC CORRELATION OF ANGUS CORE TO THE USGS #1 PORTLAND CORE

To allow comparison of our new Bridge Creek Limestone astrochronologic results with previous work from the USGS #1 Portland core, we developed a detailed correlation using carbon isotope data, carbonate content, elemental geochemistry, and bentonite stratigraphy (Sageman et al., 1997, 2006; Sageman and Lyons, 2003). The correlation is based upon a number of key chronostratigraphic markers (Fig. 3): (1) the initiation and "end of plateau" of the OAE 2 $\delta^{13}C_{org}$ excursion (e.g., Tsikos et al., 2004; Sageman et al., 2006), (2) bentonite "A" and bentonite "B" marker beds that are observed throughout the Western Interior Basin (Elder et al., 1994; the uppermost bentonite layer is near the peak of the carbon isotope profile in both cores, providing further confirmation of this correlation), (3) two broad wt% $CaCO_3$ "bundles" that follow the end of the $\delta^{13}C_{org}$ plateau at both locations, and (4) the Mn and Fe enrichment peaks observed within the OAE 2 interval. Using these chronostratigraphic markers as a guide, a detailed bed-by-bed correlation is proposed for the Bridge Creek Limestone (Fig. 3), which suggests that all of the key lithostratigraphic units are present in both sections.

The major difference between the two cores is at the base of the Bridge Creek Limestone during initiation of the OAE 2 carbon isotope excursion. Within this interval, the record is expanded into multiple lithologic couplets, instead of a massive limestone (LS1) as in the Pueblo area (Sageman et al., 2006). As will be demonstrated later herein, this reflects higher siliciclastic sedimentation rates and more continuous deposition during the initiation of OAE 2, in the Angus core.

RADIOISOTOPIC GEOCHRONOLOGY AND SEDIMENTATION RATE CONSTRAINT

Sanidines from volcanic ash in three ammonite biozones, *Watinoceras devonense*, *Euomphaloceras septemseriatum*, and *Dunveganoceras pondi*, give $^{40}Ar/^{39}Ar$ ages that are used to constrain sedimentation rates for the Bridge Creek Limestone Member and Hartland Shale Member in the Angus core (Tables 1 and 2; Meyers et al., 2012a). These specific ashes were selected based upon the precision with which they could be correlated into the core, and the small uncertainties associated with the radioisotopic ages, which produce the lowest error in derived sedimentation rate estimates. Analytical uncertainties (rather than total uncertainties) are used in the sedimentation rate assessment, as is most appropriate when evaluating the duration between stratigraphic horizons. Meyers et al. (2012a) reported the *W. devonense* age as 93.79 ± 0.12 Ma, and the *E. septemseriatum* age as 94.20 ± 0.15 Ma (95% confidence level). A new weighted mean $^{40}Ar/^{39}Ar$ age for the *D. pondi* biozone, determined here based on 25 of 33 sanidine analyses, is 95.39 ± 0.18 Ma (95% confidence level) (Fig. 4; Table 2; supplementary Table 3 [see footnote 1]). Outliers were removed from the age calculation because of "low" radiogenic $^{40}Ar^*$ (<95%) or dates that were distinguishably older than the weighted mean age and 2σ error envelope (i.e., xenocrysts). Obradovich (1993) obtained an age of 94.63 ± 0.61 Ma (95% confidence level) for this sample, relative to 28.32 Ma for the Taylor Creek sanidine standard (Duffield and Dalrymple, 1990). A recalculation of the Obradovich (1993) age using the Fish Canyon sanidine standard age of 28.201 Ma (Kuiper et al., 2008) and the Min et al. (2000) decay constant gives an age of 95.29 ± 0.61 Ma, which is statistically indistinguishable from our new age.

Calculation of sedimentation rates for the Angus core requires placement of the dated ashes within the stratigraphy. The *E. septemseriatum* ash is associated with the lowermost

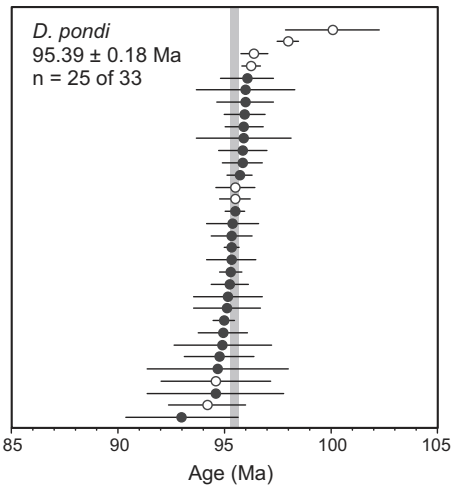

Figure 4. $^{40}Ar/^{39}Ar$ analysis for *Dunveganoceras pondi* with analytical uncertainties at the 95% confidence level. Out of 33 analyses, the 25 analyses shown as filled circles are used for calculating the weighted mean.

bentonite layer in the Bridge Creek Limestone of the Angus core (2276.75 m) and the USGS #1 Portland core (bentonite "A"; Fig. 3). In contrast, the other two ashes are not found directly within the core and thus must be placed using other lithostratigraphic and chemostratigraphic information. The *W. devonense* ash is associated with bentonite "C" in the USGS #1 Portland core (Meyers et al., 2012a) and corresponds to the interval from 2269.95 m to 2270.95 m in the Angus core based on lithostratigraphic correlation. Thus, the thickness between the biozones of *W. devonense* and *E. septemseriatum* is 6.38 ± 0.50 m, and the corresponding duration is 0.41 ± 0.19 m.y. (95% confidence level). The sedimentation rate range for this interval, given the uncertainty in both lithostratigraphic level and radioisotopic geochronology, is therefore from 0.96 to 3.12 cm/k.y. (Table 1).

The *D. pondi* biozone is located in the upper Lincoln Limestone Member in the central Western Interior (Hattin, 1975). This interval, from 2300.76 m to 2308.13 m in the Angus core, includes multiple discrete ash layers (Fig. 2). Consequently, the *D. pondi* bentonite age is placed in the middle of the interval, and one half of the thickness of the interval is taken as the placement uncertainty (3.68 m). The thickness between the *E. septemseriatum* and *D. pondi* biozones is 27.57 ± 3.68 m, while the duration is 1.19 ± 0.23 m.y. (95% confidence level). Hence, the sedimentation rate for this interval is from 1.69 to 3.28 cm/k.y. These sedimentation rates provide the nominal temporal constraints needed to test for astronomical influence using the ASM method (Meyers and Sageman, 2007).

ASTROCHRONOLOGIC RESULTS

We focus our cyclostratigraphic analysis on spatial cycles that fall within the astronomical bands, as determined by the nominal radioisotopic constraints outlined in the previous section. The spatial resolution of the XRF data is 5 mm (Nyquist frequency of 100 cycles/m), corresponding to a theoretical temporal resolution of 0.15–0.52 k.y. given the radioisotopic data. The shortest spatial cycle that could plausibly represent an astronomical signal is constrained by two factors: the lowest possible sedimentation rate (0.96 cm/k.y.), and the shortest precessional cycle (including its uncertainty; supplementary Table 2 [see footnote 1]; Laskar et al., 2004). This yields a frequency of 5.705 cycles/m (100/[0.96 cm/k.y. × 18.26 k.y.]). Here, we use 5.705 cycles/m + one Rayleigh frequency (0.143 cycles/m), which is 5.85 cycles/m, as the shortest spatial cycle tested in the ASM analyses.

The EHA and EPSA results (Figs. 5B, 5C, and 5D) reveal numerous relatively stable bedding cycles that extend throughout the Bridge Creek Limestone and into the upper Hartland Shale, especially evident in the amplitude results that have been normalized and plotted using a threshold at the 80% harmonic F-test confidence level (Fig. 5C). Within this interval, E-ASM analysis (Fig. 5D) indicates an optimal sedimentation rate of 1.51 cm/k.y. (ASM = 7.63 × 10^{-5} cycles/k.y.; H_o-SL = 0.010%; Table 3; Fig. 6) centered on the lower Bridge Creek Limestone (~2275 m), where the identified eccentricity, obliquity, and precession terms all simultaneously achieve the 90% harmonic F-test confidence level (Figs. 5C and 6F). Thus, E-ASM reveals a short stratigraphic "window" with a high signal:noise ratio, permitting an unambiguous astronomical calibration. Above and below this stratigraphic level, individual harmonic terms wax and wane in significance—nowhere else do they simultaneously coincide (Fig. 5C)—yielding an overall poorer fit to the ETP model, and consequently larger H_o-SL values. However, the general consistency of spatial bedding cycles throughout the Bridge Creek and the upper Hartland Shale (Figs. 5B–5D) is characteristic of stable sedimentation, suggesting that 1.51 cm/k.y. is an appropriate background sedimentation rate estimate for this entire interval (to ~2286 m). This sedimentation rate yields an astronomical source for all of the strong, statistically significant signals in the interval, with the exception of a stable component observed at ~1 cycle/m (Figs. 5B–5C), which calibrates to a period of ~63 k.y. (Table 3; Fig. 6F). One plausible source of the ~63 k.y. cycle is from a nonlinear response of the climate or depositional system to astronomical forcing. For example, the difference tone from interactions between O2 and E3 is ~1/62 k.y.

The middle portion of the Hartland Shale Member also demonstrates a number of relatively stable bedding cycles (Figs. 5B–5D), although the evolutive ASM results do not identify a significant result within the nominal sedimentation rate range allowed by radioisotopic geochronology (1.69–3.28 cm/k.y.). However, given the high inferred sedimentation rates through this interval, it is difficult to impossible (for sedimentation rates >1.77 cm/k.y.) to assess the long eccentricity cycle (E1) using a 7 m evolutive ASM window. Also of note, the observed bedding cycles are less stable (Fig. 5C) than those observed in the upper portion of the stratigraphy, making it more challenging to simultaneously capture the harmonic components that would result in a good fit to the ETP model (Fig. 5C). Overall, an inability to detect long eccentricity with a 7 m evolutive ASM window, and less stable spatial cycles lead to a substantial reduction in the signal:noise ratio for the middle to lower Hartland Shale Member, making astronomical cycle detection difficult.

In this portion of the stratigraphic record, where the signal:noise ratio is low, and the evolutive ASM approach has failed to identify an astronomical signal, the adaptation of the ASM method outlined in the section on "Methodology: Astrochronologic Testing" permits an alternative, rigorous test of the astronomical hypothesis. First, we isolate a 10 m section of the stratigraphy (2286–2296 m) that expresses the most stable bedding cycles in the EHA and EPSA results (Figs. 5B–5D). This yields a larger window with a greater potential for the identification of the long eccentricity term (E1). The three criteria outlined in the Astrochronologic Testing section are then used to select candidate bedding cycles for astronomical testing from the interval. Ten harmonic components are identified that satisfy these three criteria (the one exception is an 8.3 m cycle, which is too long to assess with the EHA and EPSA parameters; Fig. 6H). ASM evaluation of the 10 frequencies using the nominal sedimentation rate range of 1.69–3.28 cm/k.y. yields an optimal sedimentation rate of 2.41 cm/k.y. (ASM = 5.78 × 10^{-4} cycles/k.y.; H_o-SL = 0.157%; Table 4; Figs. 6J and 6K). Based on the observed spatial bedding frequencies in Figure 5, this sedimentation rate is proposed for the interval spanning 2286–2296 m. An astronomical signal cannot be confirmed for the lowermost Hartland Shale Member (>2296 m; shaded box in Fig. 7).

Finally, we note that the evolutive ASM results from the uppermost Lincoln Limestone Member indicate an optimal sedimentation rate of 2.13 cm/k.y. (ASM = 2.23 × 10^{-5} cycles/k.y.;

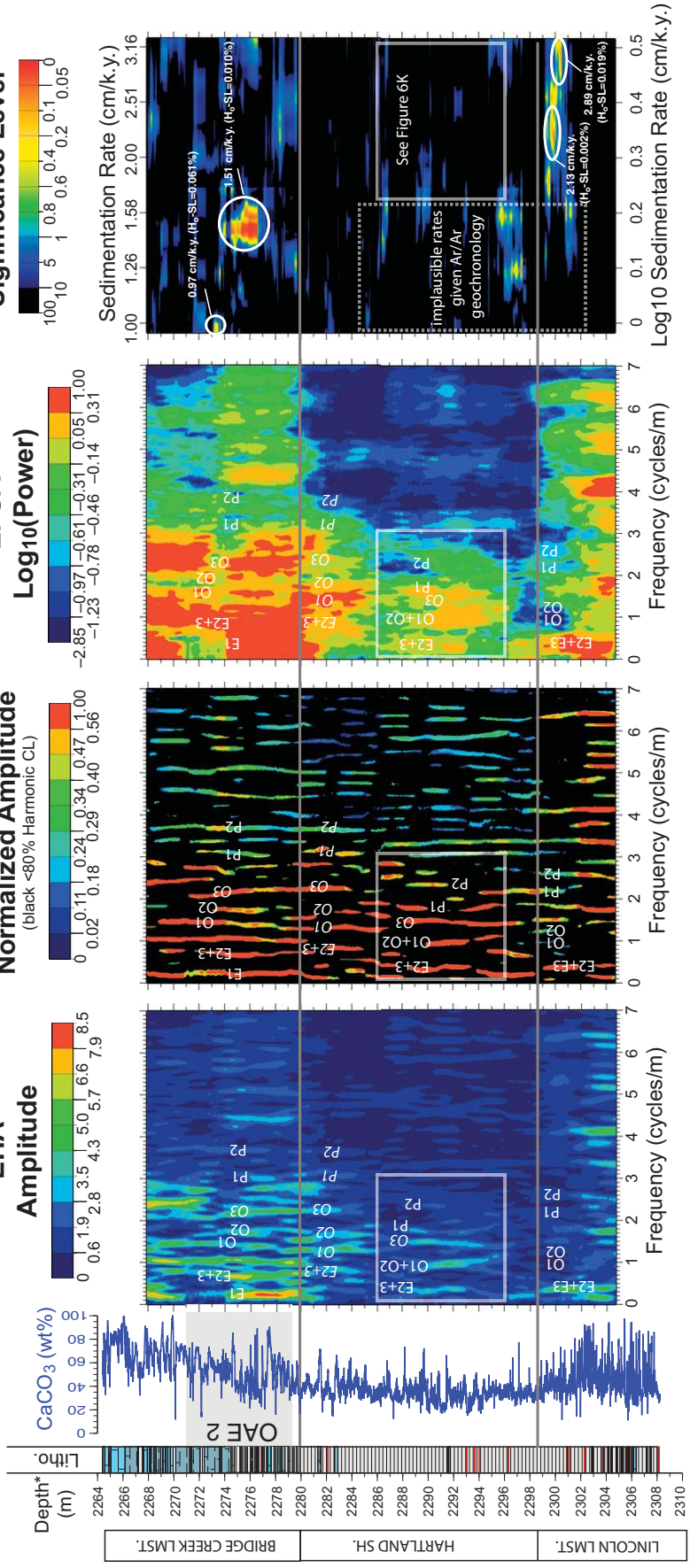

Figure 5. Time-frequency and evolutive average spectral misfit analysis results for wt% $CaCO_3$ data from the upper Lincoln Limestone, Hartland Shale, and Bridge Creek Limestone. All analyses employ three 2π discrete prolate spheroidal sequence (DPSS) tapers (Thomson, 1982) and a 7 m moving window; a linear trend was removed from each window prior to analysis. (A) Amount (wt%) $CaCO_3$. (B) Evolutive harmonic analysis (EHA) amplitude results. (C) Filtered and normalized EHA results (the maximum amplitude in each 7 m window is scaled to unity, and the results are then filtered at the 80% harmonic F-test confidence level [CL]; Meyers and Hinnov, 2010). Black indicates insignificant results. (D) Evolutive power spectral analysis results (EPSA; normalized power). (E) Evolutive average spectral misfit (ASM) results. The ASM-derived astronomical calibration is identified on parts B–D: long eccentricity (E1), short eccentricity (E2, E3), obliquity (O1, O2), and precession (P1, P2) terms. O3 indicates a short obliquity term (~29 k.y.) that was not utilized in the ASM testing. "Depth*" indicates that the thicknesses of 14 bentonites have been removed from the reported depth (in contrast to Figs. 2 and 3), with depth anchored to the top datum. OAE2—oceanic anoxic event 2. Lithology legend is the same as in Figure 2.

TABLE 3. AVERAGE SPECTRAL MISFIT (ASM)–DERIVED ASTRONOMICAL PERIODS FOR THE BRIDGE CREEK LIMESTONE WT% $CaCO_3$ DATA SERIES SPANNING 2272.5–2279.5 M IN THE ANGUS CORE, USING THE ASTRONOMICAL TARGET OF LASKAR ET AL. (2004, 2011; SEE ALSO SUPPLEMENTARY TABLE 2 [SEE TEXT FOOTNOTE 1])

Observed frequency (cycles/m)	MTM harmonic probability (%)	Observed period (k.y.)	Resolution bandwidth (k.y.)	Laskar04/Laskar11 target period (k.y.)	Misfit (cycles/k.y.)
0.2133	95.96	311.12	467.55–233.12	E1: 405.47 (415.13–396.26)	0
0.6533	95.68	101.59	114.05–91.58	E2: 126.98 (133.04–121.45)	5.308×10^{-4}
0.6533	95.68	101.59	114.05–91.58	E3: 96.91 (101.13–93.03)	0
1.0533	96.61	63.01	67.59–59.01		
1.3733	99.71	48.33	50.98–45.94	O1: 48.54 (49.33–47.79)	0
1.7200	98.91	38.59	40.26–37.05	O2: 37.66 (37.95–37.38)	0
3.0533	96.30	21.74	22.26–21.24	P1: 22.42 (23.24–21.66)	0
3.4133	98.83	19.44			
3.7067	99.35	17.91	18.26–17.57	P2: 18.33 (18.40–18.26)	3.215×10^{-6}
5.1333	95.82	12.93			
6.7867	91.34	9.78			

Note: MTM—multitaper method. Observed temporal periods were determined using an optimal sedimentation rate of ~1.51 cm/k.y.

H_o-SL = 0.002%; Fig. 5E). Given this sedimentation rate, the identified obliquity (O1, O2) terms are highly transient, although the short eccentricity (E2+E3) and P2 terms appear more stable (E1 is not detectable at this sedimentation rate using a 7 m window) (Fig. 5C). The abundance of high-amplitude signals at frequencies above the calibrated astronomical periods suggests a strong influence of nonlinear distortion processes (e.g., differential compaction/accumulation; Meyers et al., 2001) and/or other noise processes. We tentatively propose the 2.13 cm/k.y. calibration, awaiting more extensive investigation of the underlying record of the Lincoln Limestone Member.

DISCUSSION

An Extended Cenomanian-Turonian Astrochronology for the Western Interior Basin and its Comparison with Radioisotopic Geochronology

A summary of the complete astrochronologic results is shown in Figure 7, which provides a comparison with the Western Interior Basin radioisotopic geochronology and illustrates the band-pass-filtered astronomical frequencies from the wt% $CaCO_3$ data set (details of band-pass filtering are included in the figure caption). The largest uncertainty in the new ATS is for the lowermost Hartland Shale Member, where an astronomical signal has not been detected using the ASM approach (>2296 m; shaded box in Fig. 7). However, the facies preserved in the lowermost Hartland Shale are identical to those above it, and there is no observational evidence for a major discontinuity at this stratigraphic level in the Angus core, or elsewhere in the Western Interior Basin. Therefore, if the sedimentation rate for the middle Hartland Shale (2.41 cm/k.y.) is representative of the lowermost interval, and extrapolated to the top of the Lincoln Limestone Member, this suggests an ATS duration of 1230–1580 k.y. between the *E. septemseriatum* bentonite and the *D. pondi* bentonite. The range of values stems from uncertainty in the placement of the *D. pondi* bentonite in the upper Lincoln Limestone, where there are several potential correlative ash beds. The Angus core ATS result agrees well with a radioisotopic duration of 960–1420 k.y. (95% analytical uncertainty). For comparison, if the lowermost 3 m of the Hartland Shale Member is ignored in our assessment (an unrealistic, but end-member condition of instantaneous deposition), this would suggest an ATS duration of 1110–1460 k.y. for the same interval. With regards to the lower portion of the Bridge Creek Limestone, the astronomical duration between the *W. devonense* bentonite and *E. septemseriatum* bentonite is 380–450 k.y., which agrees well with a radioisotopic duration of 220–600 k.y. (95% analytical uncertainty).

The 405-k.y.-Long Eccentricity Cycle

The long eccentricity (~405 k.y.) cycle is of particular interest in most deep-time cyclostratigraphic investigations because it is considered to be the most stable of the orbital frequencies (Laskar et al., 2004, 2011). The Angus core long eccentricity band-pass filter output exhibits a strong signal in the Bridge Creek Limestone and Lincoln Limestone and a greatly diminished signal in the Hartland Shale Member. Although this attenuation could reflect a change in the primary eccentricity forcing, it may alternatively represent a threshold in the depositional system. For example, a significant increase in background clay flux during Hartland Shale deposition (Meyers et al., 2001; Sageman and Lyons, 2003) would decrease the potential for preserving astronomically forced variations in wt% $CaCO_3$ by diluting changes in carbonate content associated with productivity. The short eccentricity, obliquity, and precession band-pass filter outputs also indicate some attenuation in variability within the Hartland Shale, but this phenomenon is most pronounced for the long eccentricity signal.

Another curious aspect of the proposed long eccentricity signal is its relatively short duration in the lower Bridge Creek Limestone (ASM calibrated result of 311 k.y.) and the lower Hartland Shale (ASM calibrated result of 346 k.y.), both of which represent a perfect ASM fit given the data resolution and orbital frequency uncertainty (Tables 3 and 4). Similarly short values have also been documented for Cenomanian-Turonian strata at Deep Sea Drilling Project (DSDP) Hole 603B and Demerara Rise (Meyers et al., 2012b). Relevant to this issue, while the long eccentricity astronomical signal is most stable (Laskar et al., 2004, 2011), the preserved sedimentary record of long eccentricity can be particularly sensitive to the low-frequency stochastic noise ("red noise") that is ubiquitous in cyclostratigraphic data (Meyers, 2012). Since most of the spectral variance in strongly "red" data is at the lowest frequencies (as in Fig. 6C), this creates the unfortunate situation where an extracted band-passed signal can represent a substantial mixture of stochastic noise and orbital signal, distorting the reconstructed long eccentricity band-pass filter output (Meyers, 2012). In fact, the ASM method is designed to accommodate for this distortion in the astrochronologic testing, but it is not yet possible to directly extract the undistorted long eccentricity signal via the band-pass filtering used here.

Comparing OAE 2 Astronomical Time Scales from the Western Interior Basin

A primary purpose of this study is to test the reproducibility of the published astronomical time scale for the Cenomanian-Turonian GSSP (Meyers et al., 2001; Sageman et al., 2006). In order to provide the most objective comparison between the Angus core and Portland core chronologies, and to avoid circular reasoning, we focus on stratigraphic levels that are most strongly constrained by chemostratigraphic data and the bentonite stratigraphy. Furthermore, to avoid overinterpretation of specific stratigraphic

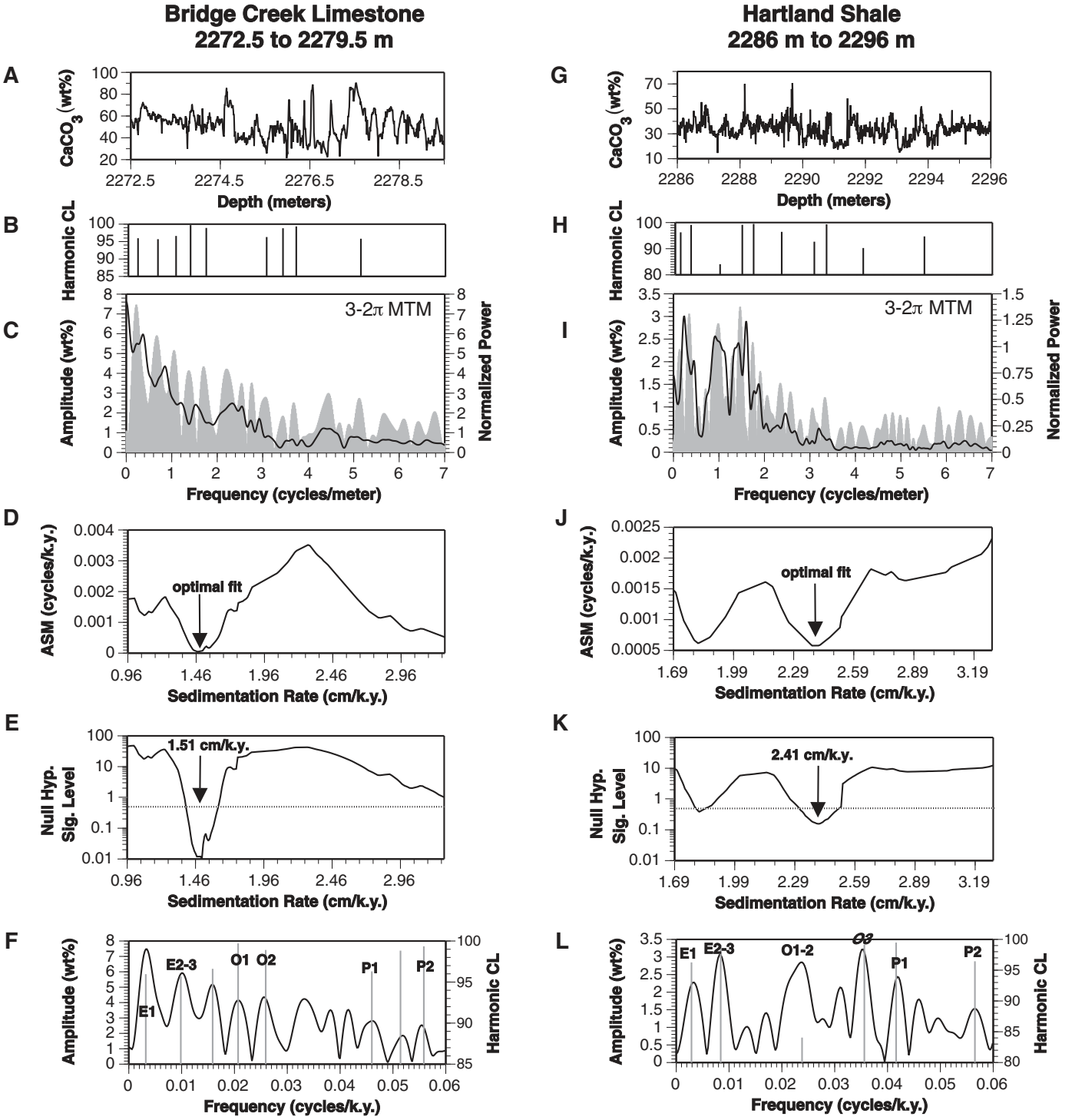

Figure 6. The average spectral misfit (ASM) results and null hypothesis test for the Bridge Creek Limestone (2272.5–2279.5 m) (A–F in the figure) and Hartland Shale (2286–2296 m) (G–L in the figure). (A, G) The wt% $CaCO_3$ profile for the interval 2272.5–2279.5 m (A) and 2286–2296 m (G). (B, H) The frequencies utilized in the ASM test, and their MTM (multitaper method) harmonic F-test confidence levels. (C, I) Three 2π DPSS (discrete prolate spheroidal sequences) MTM power spectrum (black solid line) and amplitude spectrum (shaded area). (D, J) ASM results, indicating an optimal fit at a sedimentation rate of 1.51 cm/k.y. for the Bridge Creek Limestone and 2.41 cm/k.y. for the Hartland Shale. (E, K) Null hypothesis significance levels for the ASM results, indicating lowest values at optimal sedimentation rates of 1.51 cm/k.y. for the Bridge Creek Limestone and 2.41 cm/k.y. for the Hartland Shale. Both results are below the critical significance level of 0.5% (dotted line). (F, L) The calibrated spectra based on the ASM-derived sedimentation rates, identifying long eccentricity (E1), short eccentricity (E2, E3), obliquity (O1, O2), and precession (P1, P2) terms. O3 indicates a short obliquity term (~29 k.y.) that was not utilized in the ASM testing.

TABLE 4. AVERAGE SPECTRAL MISFIT (ASM)–DERIVED ASTRONOMICAL PERIODS FOR THE HARTLAND SHALE WT% $CaCO_3$ DATA SERIES SPANNING 2286–2296 M IN THE ANGUS CORE, USING THE ASTRONOMICAL TARGET OF LASKAR ET AL. (2004, 2011; SEE SUPPLEMENTARY TABLE 2 [SEE TEXT FOOTNOTE 1])

Observed frequency (cycles/m)	MTM harmonic probability (%)	Observed period (k.y.)	Resolution bandwidth (k.y.)	Laskar04/Laskar11 target period (k.y.)	Misfit (cycles/k.y.)
0.1200	96.27	346.36	593.77–244.49	E1: 405.47 (415.13–396.26)	0
0.3500	99.1	118.75	138.55–103.91	E2: 126.98 (133.04–121.45)	0
0.3500	99.1	118.75	138.55–103.91	E3: 96.91 (101.13–93.03)	2.616×10^{-4}
0.9900	84.05	41.98	44.22–39.96	O1: 48.54 (49.33–47.79)	1.686×10^{-3}
0.9900	84.05	41.98	44.22–39.96	O2: 37.66 (37.95–37.38)	1.316×10^{-3}
1.4800	99.15	28.08	29.07–27.17		
1.7300	99.48	24.03	24.74–23.35	P1: 22.42 (23.24–21.66)	2.131×10^{-4}
2.3500	96.45	17.69	18.07–17.32	P2: 18.33 (18.40–18.26)	5.687×10^{-4}
3.0700	92.68	13.54	13.76–13.32		
3.3400	99.33	12.44	12.63–12.26		
4.1500	90.26	10.02	10.14–9.9		
5.5000	94.7	7.56	7.63–7.49		

Note: MTM—multitaper method. Observed temporal periods were determined using an optimal sedimentation rate of ~2.41 cm/k.y.

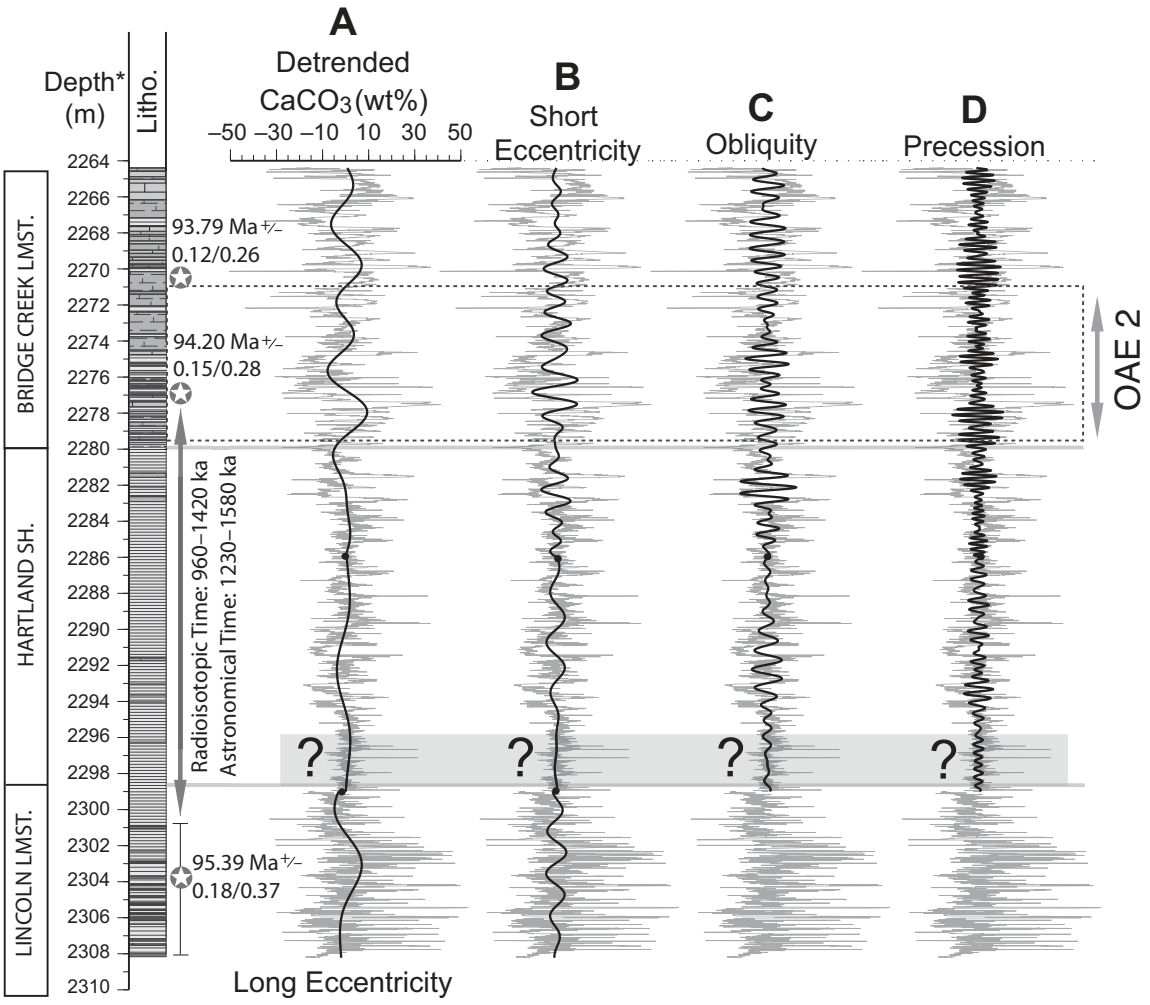

Figure 7. Band-pass filter results for the average spectral misfit (ASM)–derived astronomical components in the Angus core, which are superposed on the (piecewise) linearly detrended wt% $CaCO_3$ data set. The wt% $CaCO_3$ scale displayed in panel A also applies to panels B–D. Filtering parameters are based upon the ASM-derived sedimentation rates for three segments of the stratigraphy. 2264.4–2286 m: E1 (0.1–0.3 cycles/m), E2+3 (0.55–0.95 cycles/m), O1+2 (1.15–1.9 cycles/m), P1+2 (2.7–3.8 cycles/m). 2286–2299 m: E1 (0–0.23 cycles/m), E2+3 (0.23–0.47 cycles/m), O1+O2 (0.78–1.2 cycles/m), P1+P2 (1.62–2.46 cycles/m). 2299–2308.225 m: E1 (0–0.24 cycles/m), E2+3 (0.32–0.53 cycles/m). All filtering uses a box-car function, following linear detrending of the stratigraphic segment. Black dots identify the connecting points of the three detrended and filtered segments. "Depth*" indicates that the thicknesses of 14 bentonites have been removed from the reported depth (in contrast to Figs. 2 and 3), with depth anchored to the top datum. The shaded box at the base of the Hartland Shale Member identifies the interval for which an astronomical signal cannot be confirmed. OAE2—oceanic anoxic event 2. Lithology legend is the same as in Figure 2. Radioisotopic ages are shown with uncertainties reported in the format "analytical/total," at the 95% confidence level and 2σ, respectively.

rhythms, we utilize the objectively determined ASM-derived sedimentation rates (Figs. 5 and 6) to determine duration estimates from the Angus core.

Using the two most confident carbon isotope correlation points between the cores as an approximation for the OAE 2 interval (Figs. 3D and 3E), we find a duration of 516–613 k.y. in the Angus core, compared to 559–675 k.y. in the Portland core (Fig. 3). The range of values present in the Portland core ATS stems from uncertainties associated with sedimentation rates in the lowermost limestone bed ("LS1"; Elder, 1985) and the underlying Hartland Shale Member, for which inferences were made (Sageman et al., 2006), as well as sampling resolution of the $\delta^{13}C_{org}$ data and different options for the placement of the "end of the excursion" (Sageman et al., 2006). The range of Angus core ATS values is also due to the latter issue. It is notable that the Angus core ATS agrees well with recent OAE 2 duration estimates presented for Demerara Rise (offshore Suriname) and Tarfaya (Morocco), each of which utilizes the same evolutive ASM methodology (Meyers et al., 2012b; note that the "end of the plateau" is defined differently in the present paper). Astronomical time scales for other important sections, though, have yielded different estimates for the duration of OAE 2 (e.g., Gale et al., 1999, 2000; Voigt et al., 2008). There are many plausible reasons for such discrepancies (see "Geologic Background" section in Sageman et al., 2006), and ongoing work continues to examine this issue.

A more detailed comparison can be made by evaluating three discrete intervals within the two astrochronologies. The duration between bentonite "B" and the end of OAE 2 in the Angus core is 206–303 k.y., compared to 205–292 k.y. in the Portland core (Fig. 3). The duration between the initiation of OAE 2 and bentonite "A" in the Angus core is 167 k.y., which falls within the range of 149–178 k.y. proposed by Sageman et al. (2006; Fig. 3). Finally, the duration between the two bentonite layers in the Angus core is 143 k.y., which is 62 k.y. shorter than that in the Portland core (Fig. 3).

The observed discrepancy in duration of the bentonite A to B interval between the two cores (143 vs. 205 k.y.) could be due to three factors: correlation, hiatus, or astrochronologic methodology. Regarding the first issue, the lowermost bentonite (bentonite "A") correlates to an interval of multiple bentonite layers at other locations in the basin (Elder et al., 1994). If the bentonite "A" layer preserved in the Angus core is actually stratigraphically younger than that preserved in the Portland core, this would contribute to a difference in duration between the two sites (Fig. 3). A second possible source of discrepancy is hiatus. In fact, a hiatus of 17 k.y. was identified within the Portland core between bentonites A and B, using the Δμ EHA method (Meyers and Sageman, 2004), and this duration was added into the astronomical time scale of Sageman et al. (2006). Importantly, the overall strong astronomical cyclicity observed within the Bridge Creek Limestone of the Portland core allowed this isolated hiatus to be identified and calibrated with the Δμ EHA method (Meyers and Sageman, 2004). However, EHA results from the Angus core do not depict the expected expression of the hiatus (a bifurcation of the obliquity signal at ~2275.75 m in Figs. 5B and 5C), but this does not necessarily guarantee the absence of a hiatus, especially in records with a lower astronomical signal:noise ratio such as present in the Angus core (Meyers and Sageman, 2004). Regarding astrochronologic methodologies, the Angus core ATS was determined using an average sedimentation rate derived from a 7 m evolutive ASM analysis, while the Portland core ATS was derived using a 2 m EHA result to track the spatial frequency modulation of the short eccentricity period, followed by integration of the resultant sedimentation rate curve. Thus, it is possible for the Portland core ATS to resolve finer-scale sedimentation rate changes than those observed in the Angus core ATS. Use of the larger window in the Angus core ATS—necessitated by the overall lower signal:noise ratio as compared to the Portland core—could serve to average out and redistribute time between the three stratigraphic intervals evaluated here. The overall lower signal:noise ratio in the Angus core (a notable exception being the transition interval into OAE 2, below bentonite "A") is likely due to higher siliciclastic accumulation rates, which are also less stable. Higher background clay flux generally serves to diminish the expression of limestone beds and, in some cases, appears to have split single limestone beds (as observed in the Portland core) into two distinct beds (e.g., bed 28 in Fig. 3).

Based on the analysis presented here, we can conclude that a conservative approach for comparison of the Portland core and Angus core chronologies yields good agreement, within stated uncertainties and limitations of the astrochronologic methodologies. What is clearly unique about the Angus core ATS is the more complete preservation of bedding cycles during the initiation of OAE 2, allowing a more direct assessment of the pace of this onset, which was not as well constrained in the Portland core ATS. The time scale for OAE 2 onset is more thoroughly discussed next, including a more detailed Angus core ATS for the OAE 2 initiation that utilizes band-pass filtering guided by the ASM results.

OAE 2 Onset and the Timing of Hydrothermal Trace Metal Enrichment

The relatively stable and high rate of sedimentation during the transition from the upper Hartland Shale into the lower Bridge Creek Limestone yields a particularly strong and complete astronomical record, providing a high-resolution chronometer for the onset of OAE 2. Coupled with the new XRF data set, this presents an opportunity to better evaluate astronomical-scale environmental change and the timing of proposed hydrothermal trace metal enrichment (Orth et al., 1993; Snow et al., 2005).

The onset of Bridge Creek Limestone deposition in the Angus core is characterized by a strong precessional influence on bedding development, as illustrated by band-pass filtering (p-1 to p-9 in Fig. 8A). This is followed by attenuation of the precessional signal, but with substantial influence of obliquity (Fig. 8B; see also Meyers et al., 2012b) and short eccentricity (Fig. 8C), and also higher-frequency subprecessional variability (the latter is pronounced in the interval 2275.8–2276.8 m). To investigate the timing of proposed hydrothermal trace metal enrichment (Orth et al., 1993; Snow et al., 2005) within the context of this precessional time scale, we evaluated the Fe, Mn, and Cu XRF data sets. These specific elements were selected based on their potential for hydrothermal sources (Orth et al., 1993; Snow et al., 2005), previous documentation of their enrichment during OAE 2 in lower-resolution data sets from the Western Interior Basin (Sageman and Lyons, 2003; Snow et al., 2005), and the ability to robustly detect them with XRF scanning. Of these elements, copper displays the most scatter (supplementary Table 1 and supplementary Fig. 2 [see footnote 1]), and to accommodate for this, a Gaussian kernel (ksmooth; R Development Core Team, 2006) was used to smooth the data set.

An interval of copper, iron, and manganese enrichment is apparent in the lowermost OAE 2 interval, ~150 k.y. following the initiation of the positive carbon isotope excursion (assuming a dominant precession cycle of 22 k.y.; Fig. 8). Iron and manganese enrichment have been previously documented in the Portland core (Sageman and Lyons, 2003; Meyers et al., 2005; Meyers, 2007), and copper enrichment has been identified in the Pueblo Rock Canyon anticline section (Snow et al., 2005; unpublished data also confirm its presence in the Portland core [Stephen Meyers, 2013, personal obs.]). Elevated manganese content occurs in both carbonate-rich (arrows in Fig. 8) and carbonate-poor beds, the latter beds being coincident with iron and copper enrichment. A second, less-pronounced enrichment in copper is observed just prior to the

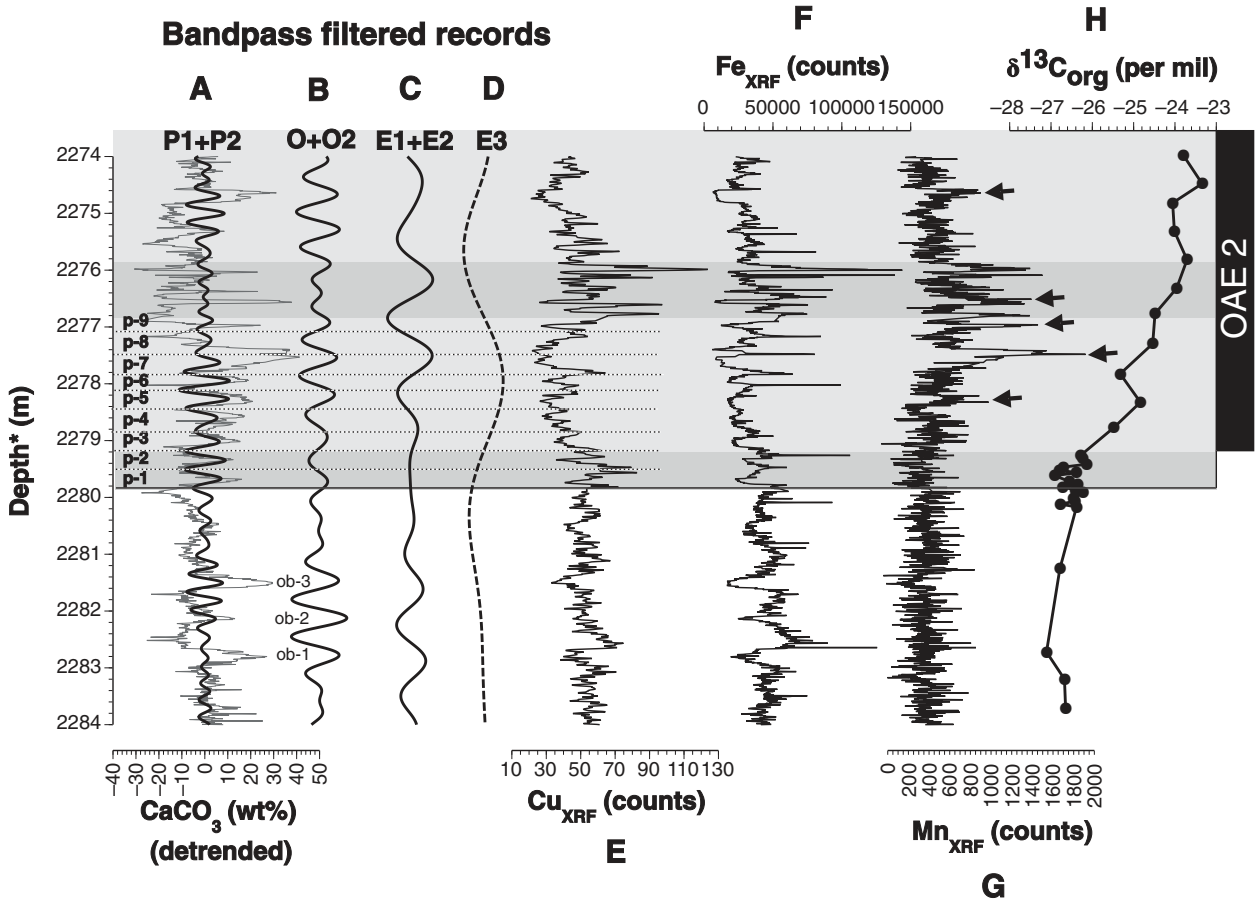

Figure 8. Detailed evaluation of the onset of oceanic anoxic event 2 (OAE 2) in the Angus core. (A) wt% $CaCO_3$ band-pass filter result for the average spectral misfit (ASM)–derived precession terms, superposed on the linearly detrended wt% $CaCO_3$ record. "p-1" to "p-9" indicate prominent precessional beats during the onset of the $\delta^{13}C_{org}$ excursion marking OAE 2. (B) wt% $CaCO_3$ band-pass filter result for the ASM-derived obliquity terms. Three strong obliquity beats prior to the OAE 2 initiation are indicated by ob-1, ob-2 and ob-3. (C) wt% $CaCO_3$ band-pass filter result for the ASM-derived short eccentricity terms. (D) wt% $CaCO_3$ band-pass filter result for the ASM-derived long eccentricity term. (E) Copper X-ray fluorescence (XRF) results (counts) from the Angus core, smoothed with a Gaussian kernel. (F) Iron XRF results (counts) from the Angus core, (G) Manganese XRF results (counts) from the Angus core. (H) Bulk organic carbon isotope data from the Angus core (‰ vs. Vienna Peedee belemnite [VPDB]; Joo et al., 2014). Please see the Figure 7 caption for information on band-pass filter parameters. "Depth*" indicates that the thicknesses of three bentonites have been removed from the reported depth (in contrast to Figs. 2 and 3), with depth anchored to the top datum.

initiation of the positive carbon isotope excursion, although a simultaneous enrichment is not apparent in the iron or manganese data (Fig. 8).

The enhanced iron and copper contents in the lower Bridge Creek Limestone have been proposed to reflect hydrothermal trace metal enrichment during OAE 2 that was associated with the formation of the Caribbean Plateau large igneous province (Larson and Erba, 1999; Leckie et al., 2002; Erba, 2004; Snow et al., 2005; Meyers, 2007). The elevated manganese concentrations are also consistent with this hydrothermal hypothesis (Snow et al., 2005). Furthermore, introduction of excess reduced compounds (Fe^{2+}, Mn^{2+}, etc.) via a magmatic event has been implicated as a primary driver of the OAE 2 (Sinton and Duncan, 1997; Leckie et al., 2002; Snow et al., 2005; Turgeon and Creaser, 2008; Elrick et al., 2009; Adams et al., 2010). Turgeon and Creaser (2008) inferred two pulses of hydrothermal activity based on osmium isotope and osmium concentration data from Demerara Rise; the first of these pulses occurs immediately prior to the initiation of the positive carbon isotope excursion at Demerara Rise, and the second follows the onset. The new geochemical data and astrochronology from the Angus core suggest that the initial pulse occurred ~20 k.y. prior to the onset of the positive carbon isotope excursion (consistent with the longest estimate of Turgeon and Creaser, 2008), with the second commencing ~170 k.y. later, over a longer sustained interval. The small magnitude of the pre-excursion copper pulse, and lack of concurrent increases in iron and manganese, may be the consequence of a more restricted Western Interior Basin at this time, and thus less efficient communication with the proto–North Atlantic and Tethys Oceans.

CONCLUSIONS

Astrochronologic testing of a new 5-mm-resolution XRF wt% $CaCO_3$ data set from the Angus core is consistent with the OAE 2 time

scale of Sageman et al. (2006), and it provides a more-continuous and expanded assessment of the onset of the event. While the Portland core ATS is judged superior for most of the Bridge Creek Limestone Member, due to the more pronounced lithologic rhythms and a larger signal:noise ratio, the onset of OAE 2 is clearly better constrained in the Angus core ATS due to expanded deposition at this site. The identification of astronomical signals in the underlying Hartland Shale and Lincoln Limestone, using evolutive ASM and a new adaptation of the approach designed for weak but pervasive signals, permits extension of the Cenomanian-Turonian time scale approximately 1 m.y. prior to the onset of the positive $\delta^{13}C_{org}$ excursion in Western Interior Basin strata. While the presence of an astronomical signal in the lowermost Hartland Shale cannot be confirmed using the ASM methodology, the observation of a strong eccentricity signal in the uppermost Lincoln Limestone Member suggests that further extension of this time scale may be feasible, which would allow a direct integration with earlier mid-Cretaceous radioisotopic data from the basin. In addition, future integration of a combined Portland core and Angus core ATS with biostratigraphic data will permit a more rigorous assessment of evolutionary rates through the late Cenomanian and early Turonian interval.

Copper, iron, and manganese XRF data from the Angus core yield evidence of the hydrothermal trace metal enrichment proposed to occur during the initiation of OAE 2. Evaluation of these data within the context of the Angus core astrochronology provides new constraints on the timing of hydrothermal activity. The unusually stable and high rate of sedimentation during the transition into OAE 2 yields a strong record of precessional forcing; thus this site represents an ideal locality for future detailed studies of hydrothermal activity and biogeochemical responses during the onset of the event, especially within the context of the Western Interior Seaway.

ACKNOWLEDGMENTS

Financial support was provided by a BP Research Assistantship to Ma and National Science Foundation grant EAR-0959108 (Meyers, Sageman, Singer). We thank Young Ji Joo (University of Oklahoma) for providing unpublished $\delta^{13}C_{org}$ and wt% $CaCO_3$ data from the Angus core, Encana Corp. for donation of the Angus core to Northwestern University, and Alan Carroll (University of Wisconsin–Madison) for comments that improved the paper.

REFERENCES CITED

Adams, D.D., Hurtgen, M.T., and Sageman, B.B., 2010, Volcanic triggering of a biogeochemical cascade during oceanic anoxic event 2: Nature Geoscience, v. 3, p. 201–204, doi:10.1038/ngeo743.

Arthur, M.A., and Dean, W.E., 1991, A holistic geochemical approach to cyclomania—Examples from Cretaceous pelagic limestone sequences, *in* Einsele, G., Ricken, W., and Seilacher, A., eds., Cycles and Events in Stratigraphy: New York, Springer-Verlag, p. 126–166.

Arthur, M.A., and Sageman, B.B., 1994, Marine black shales: Depositional mechanisms and environments of ancient deposits: Annual Review of Earth and Planetary Sciences, v. 22, p. 499–551, doi:10.1146/annurev.ea.22.050194.002435.

Arthur, M.A., Dean, W.E., Bottjer, D., and Scholle, P.A., 1984, Rhythmic bedding in Mesozoic-Cenozoic pelagic carbonate sequences: The primary and diagenetic origin of Milankovitch-like cycles, *in* Berger, A., Imbrie, J., Hays, J.D., Kukla, G., and Saltzman, B., eds., Milankovitch and Climate: Amsterdam, Netherlands, Reidel, p. 191–222.

Arthur, M.A., Dean, W.E., Pollastro, R.M., Scholle, P.A., and Claypool, G.E., 1985, A comparative geochemical study of two transgressive pelagic limestone units, Cretaceous Western Interior basin, U.S., *in* Pratt, L.M., Kauffman, E.G., and Zelt, F.B., eds., Fine-Grained Deposits and Biofacies of the Cretaceous Western Interior Seaway: Evidence of Cyclic Sedimentary Processes: Society for Sedimentary Geology (SEPM) Field Trip Guidebook 4, p. 16–27.

Arthur, M.A., Dean, W.E., and Pratt, L.M., 1988, Geochemical and climatic effects of increased marine organic carbon burial at the Cenomanian/Turonian boundary: Nature, v. 335, p. 714–717, doi:10.1038/335714a0.

Bowman, A.R., and Bralower, T.J., 2005, Paleoceanographic significance of high-resolution carbon isotope records across the Cenomanian-Turonian boundary in the Western Interior and New Jersey coastal plain, USA: Marine Geology, v. 217, p. 305–321, doi:10.1016/j.margeo.2005.02.010.

Caron, M., Robaszynski, F., Amedro, F., Baudin, F., Deconinck, J., Hochuli, P.A., Nielsen, K.S., and Tribovillard, N., 1999, Estimation de la duree de l'evenement anoxique global au passage Cenomanien/Turonien: Approche cyclostratigraphique dans la formation Bahloul en Tunisie central: Bulletin de la Société Géologique de France, v. 170, p. 145–160.

Dean, W.E., and Arthur, M.A., 1989, Iron-sulfur-carbon relationships in organic-carbon rich sequences I: Cretaceous Western Interior Seaway: American Journal of Science, v. 289, p. 708–743, doi:10.2475/ajs.289.6.708.

Dean, W.E., and Arthur, M.A., 1998, Cretaceous Western Interior Seaway Drilling Project: An overview, *in* Dean, W.E., and Arthur, M.A., eds., Stratigraphy and Paleoenvironments of the Cretaceous Western Interior Seaway, U.S.A.: Society for Sedimentary Geology (SEPM) Concepts Sedimentology and Paleontology 6, p. 1–10.

Duffield, W.A., and Dalrymple, G.B., 1990, The Taylor Creek Rhyolite of New Mexico: A rapidly emplaced field of lava domes and flows: Bulletin of Volcanology, v. 52, p. 475–487, doi:10.1007/BF00268927.

Eicher, D.L., and Diner, R., 1985, Foraminifera as indicators of water mass in the Cretaceous Greenhorn Sea, Western Interior, *in* Pratt, L.M., Kauffman, E.G., and Zelt, F.B., eds., Fine-Grained Deposits and Biofacies of the Cretaceous Western Interior Seaway: Evidence of Cyclic Sedimentary Processes: Society for Sedimentary Geology (SEPM) Field Trip Guidebook 4, p. 60–71.

Eicher, D.L., and Diner, R., 1989, Origin of the Cretaceous Bridge Creek cycles in the Western Interior, United States: Palaeogeography, Palaeoclimatology, Palaeoecology, v. 74, p. 127–146, doi:10.1016/0031-0182(89)90023-0.

Eicher, D.L., and Diner, R., 1991, Environmental factors controlling Cretaceous limestone-marlstone rhythms, *in* Einsele, G., Ricken, W., and Seilacher, A., eds., Cycles and Events in Stratigraphy: Berlin, Springer, p. 79–93.

Elder, W.P., 1985, Biotic patterns across the Cenomanian-Turonian extinction boundary near Pueblo, Colorado, *in* Pratt, L.M., Kauffman, E.G., and Zelt, F.B., eds., Fine-Grained Deposits and Biofacies of the Cretaceous Western Interior Seaway: Evidence of Cyclic Sedimentary Processes: Society for Sedimentary Geology (SEPM) Field Trip Guidebook 4, p. 157–169.

Elder, W.P., 1989, Molluscan extinction patterns across the Cenomanian-Turonian stage boundary in the Western Interior of the United States: Paleobiology, v. 15, p. 299–320.

Elder, W.P., Gustason, E.R., and Sageman, B.B., 1994, Correlation of basinal carbonate cycles to nearshore parasequences in the Late Cretaceous Greenhorn Seaway, Western Interior: Geological Society of America Bulletin, v. 106, p. 892–902, doi:10.1130/0016-7606(1994)106<0892:COBCCT>2.3.CO;2.

Elrick, M., Molina-Gaza, R., Duncan, R., and Snow, L., 2009, C-isotope stratigraphy and paleoenvironmental changes across OAE 2 (mid-Cretaceous) from shallow-water platform carbonates of southern Mexico: Earth and Planetary Science Letters, v. 277, p. 295–306, doi:10.1016/j.epsl.2008.10.020.

Erba, E., 2004, Calcareous nannofossils and Mesozoic oceanic anoxic events: Marine Micropaleontology, v. 52, p. 85–106, doi:10.1016/j.marmicro.2004.04.007.

Fischer, A.G., 1980, Gilbert bedding rhythms and geochronology, *in* Yochelson, E., ed., The Scientific Ideas of G.K. Gilbert: Geological Society of America Special Paper 183, p. 93–104.

Gale, A.S., Young, J.R., Shackleton, N.J., Crowhurst, S.J., and Wray, D.S., 1999, Orbital tuning of Cenomanian marly chalk successions: Towards a Milankovitch time-scale for the Late Cretaceous: Philosophical Transactions of the Royal Society of London, ser. A, Mathematical and Physical Sciences, v. 357, p. 1815–1829, doi:10.1098/rsta.1999.0402.

Gale, A.S., Smith, A.B., Monks, N.E.A., Young, J.A., Howard, A., Wray, D.S., and Huggett, J.M., 2000, Marine biodiversity through the late Cenomanian–early Turonian: Palaeoceanographic controls and sequence stratigraphic biases: Journal of the Geological Society of London, v. 157, p. 745–757, doi:10.1144/jgs.157.4.745.

Gale, A.S., Voigt, S., Sageman, B.B., and Kennedy, W.J., 2008, Eustatic sea-level record for the Cenomanian (Late Cretaceous)—Extension to the Western Interior Basin, USA: Geology, v. 36, p. 859–862, doi:10.1130/G24838A.1.

Gilbert, G.K., 1895, Sedimentary measurement of geologic time: The Journal of Geology, v. 3, p. 121–127, doi:10.1086/607150.

Hattin, D.E., 1975, Stratigraphy and Depositional Environment of Greenhorn Limestone (Upper Cretaceous) of Kansas: Kansas Geological Survey Bulletin 209, 128 p.

Hattin, D.E., 1986, Carbonate substrates of the Late Cretaceous Sea, central Great Plains and Southern Rocky Mountains: Palaios, v. 1, p. 347–367, doi:10.2307/3514473.

Hayes, J.M., Popp, B.N., Takigiku, R., and Johnson, M.W., 1989, An isotopic study of biogeochemical relationships between carbonates and organic matter in the Greenhorn Formation: Geochimica et Cosmochimica Acta, v. 53, p. 2961–2972, doi:10.1016/0016-7037(89)90172-5.

Hinnov, L.A., 2000, New perspectives on orbitally forced stratigraphy: Annual Review of Earth and Planetary Sciences, v. 28, p. 419–475, doi:10.1146/annurev.earth.28.1.419.

Hook, S.C., and Cobban, W.A., 1981, Late Greenhorn (Mid-Cretaceous) Discontinuity Surfaces, Southwest New Mexico: New Mexico Bureau of Mines and Mineral Resources Circular 180, p. 5–21.

Huffman, E.W.D., 1977, Performance of a new automatic carbon dioxide coulometer: Microchemical Journal, v. 22, p. 567–573, doi:10.1016/0026-265X(77)90128-X.

Jarvis, I., Gale, A.S., Jenkyns, H.C., and Pearce, M.A., 2006, Secular variation in Late Cretaceous carbon isotopes: A new $\delta^{13}C$ reference curve for the Cenomanian-Santonian (99.6–83.5 Ma): Geological Magazine, v. 143, p. 561–608, doi:10.1017/S0016756806002421.

Joo, Y.J., Sageman, B.B., and Hurtgen, M.T., 2014, Cenomanian to Campanian carbon isotope record from the Western Interior Basin: Journal of Sedimentary Research (in press).

Kauffman, E.G., 1977, Geological and biological overview: Western Interior Cretaceous Basin: The Mountain Geologist, v. 13, p. 75–99.

Kuhnt, W., Nederbragt, A., and Leine, L., 1997, Cyclicity of Cenomanian-Turonian organic-carbon–rich sediments in the Tarfaya Atlantic Coastal Basin (Morocco): Cretaceous Research, v. 18, p. 587–601, doi:10.1006/cres.1997.0076.

Kuhnt, W., Luderer, F., Nederbragt, S., Thurow, J., and Wagner, T., 2004, Orbital-scale record of the late Cenomanian–Turonian oceanic anoxic event (OAE-2) in the Tarfaya Basin (Morocco): International Journal of Earth Sciences, v. 94, p. 147–159, doi:10.1007/s00531-004-0440-5.

Kuiper, K.F., Deino, A., Hilgen, F.J., Krijgsman, W., Renne, P.R., and Wijbrans, J.R., 2008, Synchronizing rock clocks of Earth history: Science, v. 320, p. 500–504, doi:10.1126/science.1154339.

Kuypers, M.M.M., Lourens, L.J., Rijpstra, W.I.C., Pancost, R.D., Nijenhuis, I.A., and Sinninghe Damste, J.S., 2004, Orbital forcing of organic carbon burial in the proto–North Atlantic during oceanic anoxic event 2: Earth and Planetary Science Letters, v. 228, p. 465–482, doi:10.1016/j.epsl.2004.09.037.

Larson, R.L., and Erba, E., 1999, Onset of the mid-Cretaceous greenhouse in the Barremian-Aptian: Igneous events and the biological, sedimentary, and geochemical responses: Paleoceanography, v. 14, p. 663–678, doi:10.1029/1999PA900040.

Laskar, J., Robutel, P., Joutel, F., Gastineau, M., Correia, A.C.M., and Levrard, B., 2004, A long-term numerical solution for the insolation quantities of the Earth: Astronomy & Astrophysics, v. 428, p. 261–285, doi:10.1051/0004-6361:20041335.

Laskar, J., Fienga, A., Gastineau, M., and Manche, H., 2011, La2010: A new orbital solution for the long-term motion of the Earth: Astronomy & Astrophysics, v. 532, p. A89, doi:10.1051/0004-6361/201116836.

Leckie, R.M., Bralower, T.J., and Cashman, R., 2002, Oceanic anoxic events and plankton evolution: Biotic response to tectonic forcing during the mid-Cretaceous: Paleoceanography, v. 17, p. 1–29, doi:10.1029/2001PA000623.

Li, X., Jenkyns, H.C., Wang, C., Hu, X., Chen, X., Wei, Y., Huang, Y., and Cui, J., 2006, Upper Cretaceous carbon- and oxygen-isotope stratigraphy of hemipelagic carbonate facies from southern Tibet, China: Journal of the Geological Society of London, v. 163, p. 375–382, doi:10.1144/0016-764905-046.

Locklair, R.E., and Sageman, B.B., 2008, Cyclostratigraphy of the Upper Cretaceous Niobrara Formation, Western Interior, U.S.A.: A Coniacian-Santonian orbital timescale: Earth and Planetary Science Letters, v. 269, p. 540–553, doi:10.1016/j.epsl.2008.03.021.

Malinverno, A., Erba, E., and Herbert, T.D., 2010, Orbital tuning as an inverse problem: Chronology of the early Aptian oceanic anoxic event 1a (Selli level) in the Cismon APTICORE: Paleoceanography, v. 25, PA2203, doi:10.1029/2009PA001769.

Meyers, S.R., 2007, Production and preservation of organic matter: The significance of iron: Paleoceanography, v. 22, PA4211, doi:10.1029/2006PA001332.

Meyers, S.R., 2012, Seeing red in cyclic stratigraphy: Spectral noise estimation for astrochronology: Paleoceanography, v. 27, PA3228, doi:10.1029/2012PA002307.

Meyers, S.R., and Hinnov, L.A., 2010, Northern Hemisphere glaciation and the evolution of Plio-Pleistocene climate noise: Paleoceanography, v. 25, PA3207, doi:10.1029/2009PA001834.

Meyers, S.R., and Sageman, B.B., 2004, Detection, quantification, and significance of hiatuses in pelagic and hemipelagic strata: Earth and Planetary Science Letters, v. 224, p. 55–72, doi:10.1016/j.epsl.2004.05.003.

Meyers, S.R., and Sageman, B.B., 2007, Quantification of deep-time orbital forcing by average spectral misfit: American Journal of Science, v. 307, p. 773–792, doi:10.2475/05.2007.01.

Meyers, S.R., Sageman, B., and Hinnov, L., 2001, Integrated quantitative stratigraphy of the Cenomanian-Turonian Bridge Creek Limestone Member using evolutive harmonic analysis and stratigraphic modeling: Journal of Sedimentary Research, v. 71, p. 628–644, doi:10.1306/012401710628.

Meyers, S.R., Sageman, B.B., and Lyons, T., 2005, Organic carbon burial rate and the molybdenum proxy: Theoretical framework and application to Cenomanian-Turonian OAE II: Paleoceanography, v. 20, PA2002, doi:10.1029/2004PA001068.

Meyers, S.R., Sageman, B.B., and Pagani, M., 2008, Resolving Milankovitch: Consideration of signal and noise: American Journal of Science, v. 308, p. 770–786, doi:10.2475/06.2008.02.

Meyers, S.R., Siewert, S.E., Singer, B.S., Sageman, B.B., Condon, D.J., Obradovich, J.D., Jicha, B.R., and Sawyer, D.A., 2012a, Intercalibration of radioisotopic and astrochonologic time scales for the Cenomanian-Turonian boundary interval, Western Interior Basin, USA: Geology, v. 40, p. 7–10, doi:10.1130/G32261.1.

Meyers, S.R., Sageman, B.B., and Arthur, M.A., 2012b, Obliquity forcing of organic matter accumulation during oceanic anoxic event 2: Paleoceanography, v. 27, PA3212, doi:10.1029/2012PA002286.

Min, K., Mundil, R., Renne, P.R., and Ludwig, K.R., 2000, A test for systematic errors in $^{40}Ar/^{39}Ar$ geochronology through comparison with U/Pb analysis of a 1.1-Ga rhyolite: Geochimica et Cosmochimica Acta, v. 64, p. 73–98, doi:10.1016/S0016-7037(99)00204-5.

Obradovich, J., 1993, A Cretaceous time scale, *in* Caldwell, W.G.E., and Kauffman, E.G., eds., Evolution of the Western Interior Basin: Geological Society of Canada Special Paper 39, p. 379–396.

Orth, C.J., Attrep, M., Quintana, L.R., Elder, W.P., Kauffman, E.G., Diner, R., and Villamil, T., 1993, Elemental abundance anomalies in the late Cenomanian extinction interval: A search for the source(s): Earth and Planetary Science Letters, v. 117, p. 189–204, doi:10.1016/0012-821X(93)90126-T.

Paul, C.R.C., Lamolda, M.A., Mitchell, S.F., Vaziri, M.R., Gorostidi, A., and Marshall, J.D., 1999, The Cenomanian-Turonian boundary at Eastbourne (Sussex, UK): A proposed European reference section: Palaeogeography, Palaeoclimatology, Palaeoecology, v. 150, p. 83–121, doi:10.1016/S0031-0182(99)00009-7.

Potts, P.J., Tindle, A.G., and Webb, P.C., 1992, Geochemical Reference Material Compositions: Rocks, Minerals, Sediments, Soils, Carbonates, Refractories & Ores Used in Research & Industry: Caithness, UK, Whittles Publishing, 313 p.

Pratt, L.M., 1985, Isotopic studies of organic matter and carbonate in rocks of the Greenhorn marine cycle, *in* Pratt, L.M., Kauffman, E.G., and Zelt, F.B., eds., Fine-Grained Deposits and Biofacies of the Cretaceous Western Interior Seaway: Evidence of Cyclic Sedimentary Processes: Society for Sedimentary Geology (SEPM) Field Trip Guidebook 4, p. 38–48.

Pratt, L.M., Arthur, M.A., Dean, W.E., and Scholle, P.A., 1993, Paleoceanographic cycles and events during the Late Cretaceous in the Western Interior Seaway of North America, *in* Caldwell, W.G.E., and Kauffman, E.G. eds., Evolution of the Western Interior Basin: Geological Association of Canada Special Paper 39, p. 333–354.

Premoli-Silva, I., Erba, E., Salvini, G., Verga, D., and Locatelli, C., 1999, Biotic changes in Cretaceous anoxic events: Journal of Foraminiferal Research, v. 29, p. 352–370.

Prokoph, A., Villeneuve, M., Agterberg, F.P., and Rachold, V., 2001, Geochronology and calibration of global Milankovitch cyclicity at the Cenomanian-Turonian boundary: Geology, v. 29, p. 523–526, doi:10.1130/0091-7613(2001)029<0523:GACOGM>2.0.CO;2.

R Development Core Team, 2006, R: A Language and Environment for Statistical Computing: Vienna, Austria, R Foundation for Statistical Computing, http://www.R-project.org.

Richter, T.O., van der Gaast, S., Koster, B., Vaars, A., Gieles, R., de Stigter, H.C., and van Weering, T.C.E., 2006, The Avaatech XRF core scanner: Technical description and applications to NE Atlantic sediments, *in* Rothwell, R.G., ed., New Techniques in Sediment Core Analysis: Geological Society of London Special Publication 267, p. 39–50.

Roberts, L.N.R., and Kirschbaum, M.A., 1995, Paleogeography of the Late Cretaceous of the Western Interior of Middle North America—Coal Distribution and Sediment Accumulation: U.S. Geological Survey Professional Paper 1561, 115 p.

Sageman, B.B., 1996, Lowstand tempestites: Depositional model for Cretaceous skeletal limestones, Western Interior: Geology, v. 24, p. 888–892, doi:10.1130/0091-7613(1996)024<0888:LTDMFC>2.3.CO;2.

Sageman, B.B., and Lyons, T., 2003, Geochemistry of fine-grained sediments and sedimentary rocks, *in* Holland, H.D., and Karl K.T., eds., Treatise on Geochemistry: Amsterdam, Netherlands, Elsevier, p. 115–158.

Sageman, B.B., Rich, J., Arthur, M.A., Birchfield, G.E., and Dean, W.E., 1997, Evidence for Milankovitch periodicities in Cenomanian-Turonian lithologic and geochemical cycles: Western Interior, U.S.: Journal of Sedimentary Research, v. 67, p. 286–301.

Sageman, B., Rich, J., Savrda, C.E., Bralower, T., Arthur, M.A., and Dean, W.E., 1998, Multiple Milankovitch cycles in the Bridge Creek Limestone (Cenomanian-Turonian), Western Interior Basin, *in* Arthur, M.A., and Dean, W.E., eds., Stratigraphy and Paleoenvironments of the Cretaceous Western Interior Seaway, USA: Society of Sedimentary Geology Concepts in Sedimentology and Paleontology 6, p. 153–171.

Sageman, B.B., Meyers, S.R., and Arthur, M.A., 2006, Orbital timescale for the Cenomanian-Turonian boundary stratotype and OAE II, central Colorado, USA: Geology, v. 34, p. 125–128, doi:10.1130/G22074.1.

Sageman, B.B., Singer, B.S., Meyers, S.R., Siewert, S.E., Walaszczyk, I., Condon, D.J., Jicha, B.R., Obradovich, J.D., and Sawyer, D.A., 2014, Integrating $^{40}Ar/^{39}Ar$, U-Pb, and astronomical clocks in the Cretaceous Niobrara Formation, Western Interior Basin, USA: Geological Society of America Bulletin (in press), doi:10.1130/B30929.

Schlanger, S.O., Arthur, M.A., Jenkyns, H.C., and Scholle, P.A., 1987, The Cenomanian-Turonian oceanic anoxic event: I. Stratigraphy and distribution of organic carbon–rich beds and the marine $\delta^{13}C$ excursion, *in* Brooks, J., and Fleet, A.J., eds., Marine Petroleum Source Rocks: Geological Society of London Special Publication 26, p. 371–399.

Schmitz, M.D., 2012, Radiogenic Isotope Geochronology: Amsterdam, Netherlands, Elsevier, p. 115–126, doi:10.1016/B978-0-444-59425-9.00006-8.

Sinton, C.W., and Duncan, R.A., 1997, Potential links between ocean plateau volcanism and global ocean anoxia at the Cenomanian-Turonian boundary: Economic Geology and the Bulletin of the Society of Economic Geologists, v. 92, p. 836–842, doi:10.2113/gsecongeo.92.7-8.836.

Snow, L.J., Duncan, R.A., and Bralower, T.J., 2005, Trace element abundances in the Rock Canyon anticline, Pueblo, Colorado, marine sedimentary section and their relationship to Caribbean plateau construction and oxygen anoxic event 2: Paleoceanography, v. 20, PA3005, doi:10.1029/2004PA001093.

Thomson, D.J., 1982, Spectrum estimation and harmonic analysis: IEEE Proceedings, v. 70, p. 1055–1096, doi:10.1109/PROC.1982.12433.

Tsikos, H., Jenkyns, H.C., Walsworth-Bell, B., Petrizzo, M.R., Forster, A., Kolonic, S., Erba, E., Premoli Silva, I., Baas, M., Wagner, T., and Sinninghe Damsté, J.S., 2004, Carbon-isotope stratigraphy recorded by the Cenomanian-Turonian oceanic anoxic event: Correlation and implications based on three key localities: Journal of the Geological Society of London, v. 161, p. 711–719, doi:10.1144/0016-764903-077.

Turgeon, S.C., and Creaser, R.A., 2008, Cretaceous oceanic anoxic event 2 triggered by a massive magmatic episode: Nature, v. 454, p. 323–326, doi:10.1038/nature07076.

Voigt, S., Erbacher, J., Mutterlose, J., Weiss, W., Westerhold, T., Wiese, F., Wilmsen, M., and Wonik, T., 2008, The Cenomanian-Turonian of the Wunstorf section (North Germany): Global stratigraphic reference section and new orbital time scale for Oceanic Anoxic Event 2: Newsletters on Stratigraphy, v. 43, p. 65–89.

Wang, C., Hu, X., Jansa, L., Wan, X., and Tao, R., 2001, The Cenomanian-Turonian anoxic event in southern Tibet: Cretaceous Research, v. 22, p. 481–490, doi:10.1006/cres.2001.0271.

Weedon, G.P., 2003, Time-Series Analysis and Cyclostratigraphy: Cambridge, UK, Cambridge University Press, 276 p.

Science Editor: Christian Koeberl
Associate Editor: Kenneth G. MacLeod

Manuscript Received 5 May 2013
Revised Manuscript Received 17 January 2014
Manuscript Accepted 11 February 2014

Printed in the USA